Draft version January 25, 2024
Typeset using LaTeX **modern** style in AASTeX631

`nuance`: Efficient detection of planets transiting active stars

Lionel J. Garcia,[1] Daniel Foreman-Mackey,[1] Dax L. Feliz,
Catriona A. Murray, and Francisco J. Pozuelos

[1] *Center for Computational Astrophysics, Flatiron Institute, New York, NY, USA*

ABSTRACT

We present *nuance*, an algorithm to search for planetary transits in light curves featuring correlated noise, such as instrumental signals and stellar photometric variability. To deal with this noise, a common approach consists in cleaning a light curve from nuisance signals before searching for transits. However, we show that this approach limit the detection efficiency of traditional techniques. As this effect depends on the correlated noise characteristics, we map the relevant parameter space for which transits are altered, and quantify the detection efficiency limits on a set of simulated light curves. On this synthetic dataset, we show that *nuance* largely outperforms the detection capabilities of a commonly used transit search technique, which consists in cleaning light curves from stellar variability with an optimal bi-weight filter before searching for transits using a box-least-square algorithm. Then, in order to assess the performance of *nuance* on real datasets, we inject and recover transits into the TESS light curves of 438 M dwarfs, and compare our method to 4 detrending techniques followed by a Box-Least-Square search. For transits with a duration exceeding one fifth of the stellar variability timescale, we show that *nuance*is the most performant in 94% of cases, leading to both the highest number of true positives and the lowest number of false positive detections. Although simultaneously searching for transits while modeling correlated noise is expected to be computationally expensive, we make our algorithm tractable and available as the JAX-powered Python package nuance, allowing its use on distributed environments and GPU devices. Finally, we explore the prospects offered by the *nuance* formalism, and its use to advance our knowledge of active stars and their transiting exoplanets, both using space-based and sparse ground-based observations.

Keywords: transit search, exoplanets, stellar activity, time series analysis, Gaussian processes

Corresponding author: Lionel J. Garcia
lgarcia@flatironinstitute.org

INTRODUCTION

Transiting exoplanets are keystone objects for the field of exoplanetary science, but detecting transits in light curves featuring stellar variability and instrumental signals remains a challenge (Pont et al. 2006; Howell et al. 2016). For this reason, known transiting exoplanets tend to be found around quieter stars, or belong to the population of close-in giants whose transit signals dominate over stellar rotational variability (Simpson et al. 2023). However, transiting exoplanets around active stars are discoveries with significant scientific value. First, as younger stars are more active (Skumanich 1972), being able to detect planets transiting active stars will favor the discovery of young planetary systems (e.g. Newton et al. 2022). Second, as stellar variability may originate from surface active regions (such as starpots), transiting exoplanets can be used to map the photosphere of active stars (e.g. Morris et al. 2017), benefiting both the study of stellar atmospheres and the concerning impact of their non-uniformity on planetary atmosphere retrievals (Rackham et al. 2018). Overall, enabling the detection of transits in light curves with high levels of correlated noises will greatly benefit the study of terrestrial exoplanets around late M-dwarfs, usually observed at lower SNR and more likely to display photometric variability (e.g. Murray et al. 2020).

Commonly used transit-search algorithms, such as the Box-Least-Square algorithm (BLS, Kovács et al. 2002) are capable of detecting transits in light curves containing only transit signals and white noise. Using this method, the simplest way to detect transits in a light curve featuring correlated noise (either astrophysical or instrumental), is to first clean it from nuisance signals before performing the search. This strategy is widely adopted by the community, both using physically-motivated systematic models like Luger et al. (2016, 2018), or filtering techniques (Jenkins et al. 2010, Hippke et al. 2019). However, when correlated noise starts resembling transits, this cleaning step (often referred to as *detrending*) is believed to degrade their detectability (see subsection 4.3 of Hippke et al. 2019). In this case, the only alternative to search for transits is to perform a full-fledged modeling of the light curve, including both transits and correlated noise, and to compute the likelihood of the data to the transit model on a wide parameter space, an approach largely avoided due to its intractable nature. Nonetheless, Kovács et al. (2016) ask: *Periodic transit and variability search with simultaneous systematics filtering: Is it worth it?*. The latter study explores a handful of cases and generally discards the benefit of using a full-fledged approach.

In this paper, we identify regions of light curves morphological parameter space for which a full-fledged transit search is necessary, and we present *nuance*[1], a method

[1] Throughout the paper, *nuance* written in italics refers to the algorithmic and analytical method, while nuance in sans-serif refers to its implementation.

to search for transit signals while simultaneously modeling correlated noises in a tractable way. In section 1, we describe the effect of correlated noise on transit light curves and the effect of its detrending on transit signals detectability. In section 2, we present *nuance*, and the two main steps on which this method is based: the linear search and the periodic search. In section 3, we test the performance of *nuance* on a wide variety of cases, and compare our method to commonly used transit search algorithms. This include transits injected in synthetic datasets, but also in the TESS light curves of 438 rapidly-rotating M dwarfs. Finally, in section 4, we discuss the results and the limitations of *nuance*, and we conclude in section 5.

1. MOTIVATION

A strong assumption when using the BLS algorithm to search for transits is that the searched dataset only contains transit signals and white noise, justifying the need for detrending. In this section, we explore this effect by simulating light curves containing a transit signal and correlated noise in the form of stellar variability, and study how detrending the latter affects the transit signal detectability depending on the light curve morphological characteristics. Hence, we first present how transit light curves are simulated, using a stochastic model of stellar variability, and describe the detection metric we employ to quantify transit detectability in the presence of correlated noise.

1.1. *Light curve simulations*

To perform this study, we want to simulate realistic light curves that contain instrumental signals, transit signals and correlated noise with characteristics that can be controlled using a set of interpretable parameters. To this end, we model light curves as realizations of a Gaussian Process (GP; Rasmussen & Williams 2005) with a mean containing the instrumental and transit signals, and a kernel allowing to model different forms of correlated noise controlled by its hyperparameters.

Let f be the simulated differential flux of a star sampled and arranged in the vector $\boldsymbol{f}$ associated to the vector of times $\boldsymbol{t}$, such that

$$\boldsymbol{f} \sim \mathcal{N}(\boldsymbol{\mu}, \boldsymbol{C}),$$

i.e. that $\boldsymbol{f}$ is drawn from a GP of mean $\boldsymbol{\mu}$ and covariance matrix $\boldsymbol{C}$. For practical reasons, we model $\boldsymbol{\mu}$ as a linear combination of M explanatory variables, such that

$$\boldsymbol{\mu} = \boldsymbol{X}\boldsymbol{w} \tag{1}$$

where the first $M-1$ columns of $\boldsymbol{X}$ are contemporaneous instrumental time series measurements, such as the position of the star on the detector or the sky background (e.g.), and its last column is a box-shaped transit signal with a fixed epoch, duration and period. This way, the transit signal is part of the mean linear model, meaning that once the design matrix $\boldsymbol{X}$ is constructed the transit is only parametrized by its depth Δ.

As we are interested in correlated noise in the form of stellar variability, we choose a physically-motivated GP kernel to model the covariance matrix $\boldsymbol{C}$, describing stellar variability through the covariance of a stochastically-driven damped harmonic oscillator (SHO, Foreman-Mackey et al. 2017; Foreman-Mackey 2018) parametrized by its quality factor Q, its pulsation ω and the amplitude of the kernel function σ (the full expression of the kernel function is provided in section A.3). This choice of mean and kernel function completely defines the GP, from which light curves with different levels of correlated noise can be drawn (see an example in Figure 18).

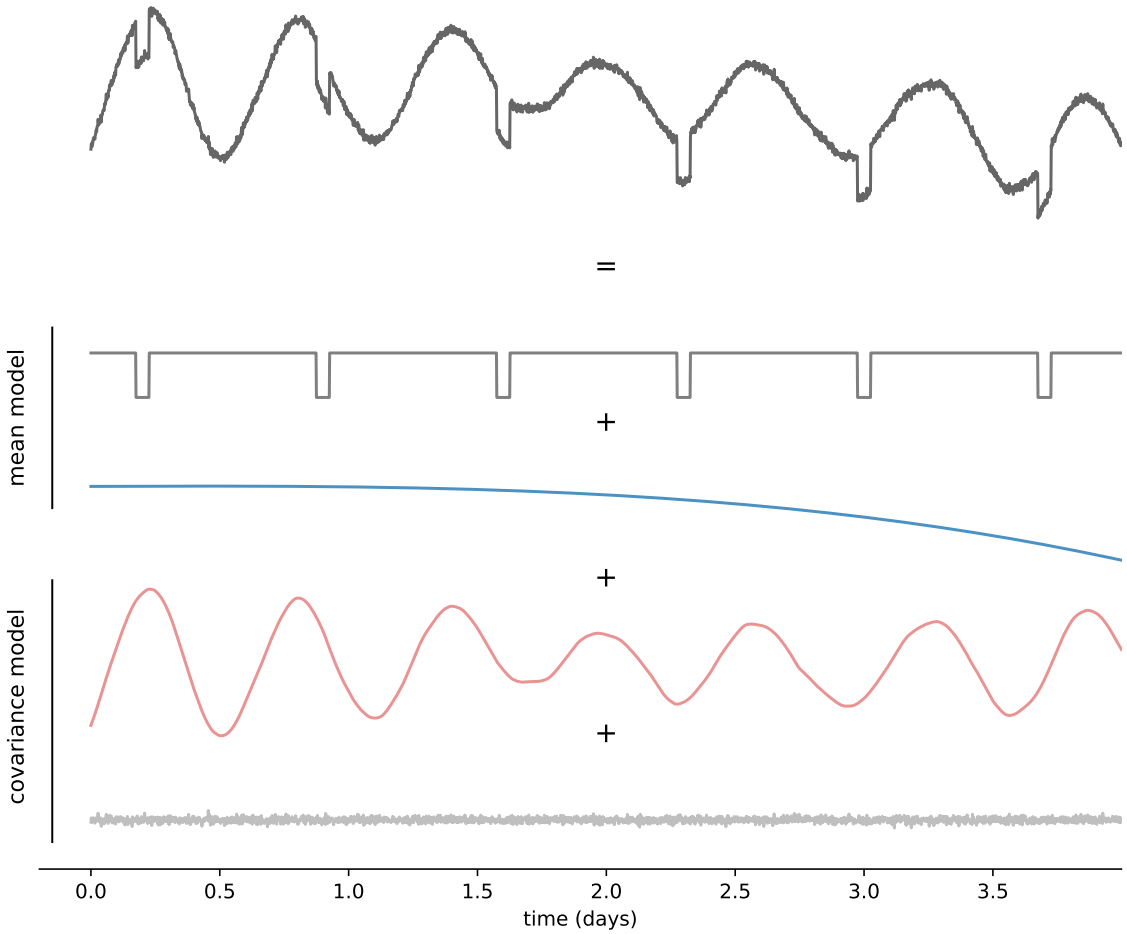

Figure 1. Flux times series drawn from the GP model described in section 1.1. This dataset corresponds to an observation of 4 days with an exposure time of 2 minutes. The mean of this signal consists in a periodic transit signal of period $P = 0.7$ days, duration $D = 1.2$ hours and depth $\Delta = 0.02$ (dark gray) plus an instrumental signal (blue). Correlated noise in the form of stellar variability is simulated with an SHO kernel of hyperparameters $\omega = \pi/6D$, $Q = 45$ and $\sigma = \Delta$. Finally, white noise with a standard deviation of 0.001 is added to the diagonal of the covariance matrix.

1.2. *Transit detectability*

One way to quantify the detectability of a unique transit signal is to compute its signal-to-noise-ratio expressed as

$$SNR = \frac{\Delta}{\sigma}\sqrt{n},$$

where Δ is the transit depth, σ the measurements uncertainty (assuming homoscedasticity), and n the number of points within transit. Although this metric is useful to assess the strength of the transit signal given a certain photometric precision, it does not account for the presence of correlated noise. However, instrumental and other astrophysical signals will necessarily affect the detectability of transits in realistic

light curves (Pont et al. 2006). For this reason, the combined differential photometric precision metric was developed (CDPP; Jenkins et al. 2010), and used in the context of the Kepler mission to assess the level of correlated noise in light curves, affecting the detectability of transits with a given duration. The CDPP is computed by decomposing the data in the time-frequency domain using wavelets, and measures the significance of a distorted transit signal in the whitened data. For a given transit duration, the CDPP is then a measure of the noise remaining after filtering the light curve in each frequency band, taking into account the presence of non-stationary correlated noise of a given timescale (see Jenkins et al. 2010 for more details). Hence, we can estimate the significance of the transit signal accounting for the presence of correlated noise as

$$SNR = \frac{\hat{\Delta}}{CDPP_D}, \tag{2}$$

where $CDPP_D$ is the CDPP computed for a given transit duration D and $\bar{\Delta}$ is the transit depth after detrending. For simplicity, the CDPP is computed using the method from Gilliland et al. (2011) implemented in the lightkurve Python package (Lightkurve Collaboration et al. 2018) and $\hat{\Delta}$ is the depth obtained by solving Equation 1 with the last column of $\boldsymbol{X}$ containing a normalized transit model. Figure 2 shows the SNR from Equation 2 computed for a unique transit observed in the absence (grey) and presence of correlated noise (red).

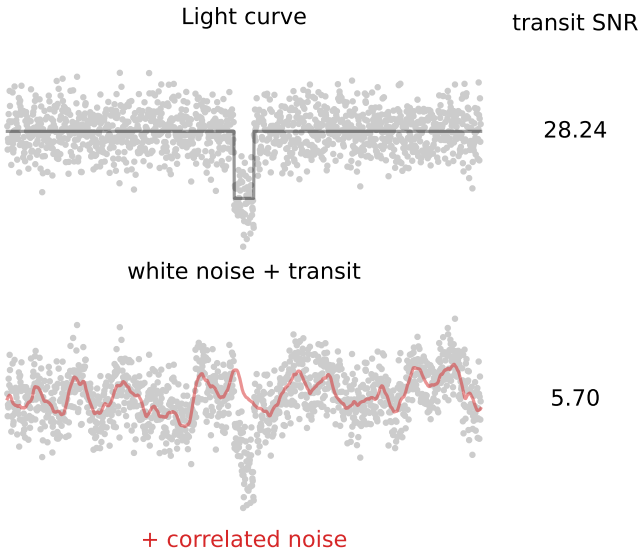

Figure 2. Illustration of the effect of correlated noise on a single transit SNR. An hour-long transit of depth 0.01 is generated on top of white noise (standard deviation of 0.0015) as part of a 24-hours observation with an exposure time of 1 minute (top). Then, in the bottom plot, correlated noise is added, generated using a GP with an SHO kernel of hyperparameters $\omega = 60$, $Q = 0.5$ and $\sigma = \Delta/4$. The SNR on the right of each light curve is computed using Equation 2. Models used to simulate these data are provided in Appendix A.

As illustrated in Figure 2, the presence of correlated noise strongly decreases the transit signal SNR, which would ultimately limit its detectability.

1.3. *Detrending methods and their effects*

The presence of instrumental correlated noise motivated the development of systematics detrending algorithms, such as the Trend Filtering Algorithm (TFA, Kovács et al. 2005, in its primary use case), SysRem (Tamuz et al. 2005) or Pixel Level Decorrelation (PLD, Deming et al. 2015; see also Everest from Luger et al. 2016, 2018). Most of these methods rely on the shared nature of instrumental signals among light curves (or neighboring pixels) such that the correction applied should not degrade the transit signal and can be modeled using contemporaneous measurements (e.g. detector's temperature, pointing error, sky background or airmass time series). But even after instrumental signals have been removed, stellar variability and other astrophysical signals remain, which gave rise to several approaches. Some of them are physically-motivated and make use of GPs (e.g. Aigrain et al. 2016), others are empirical and make use of filtering and data-driven algorithms (Jenkins et al. 2010, Hippke et al. 2019). In this section, we show how these techniques impact transits detectability, depending on the morphological characteristics of light curves.

In Figure 3, we simulate a transit signal on top of which we add photometric stellar variability with different timescales, sampled from a GP with an SHO kernel described in section A.3. For each light curve, we reconstruct and detrend stellar variability in two ways: one using the widely-adopted Tukey's bi-weight filter, presented in Mosteller & Tukey (1977) and using the implementation from wõtan[2] (Hippke et al. 2019); the other using the same GP from which the data has been sampled. We then estimate the resulting transit depth and compute the remaining transit SNR using Equation 2. Figure 3 clearly shows the effect of both detrending techniques on transits SNR, and intuitively suggests that this degradation due to detrending is strongly dependent on the correlated noise characteristics encountered.

[2] https://github.com/hippke/wotan

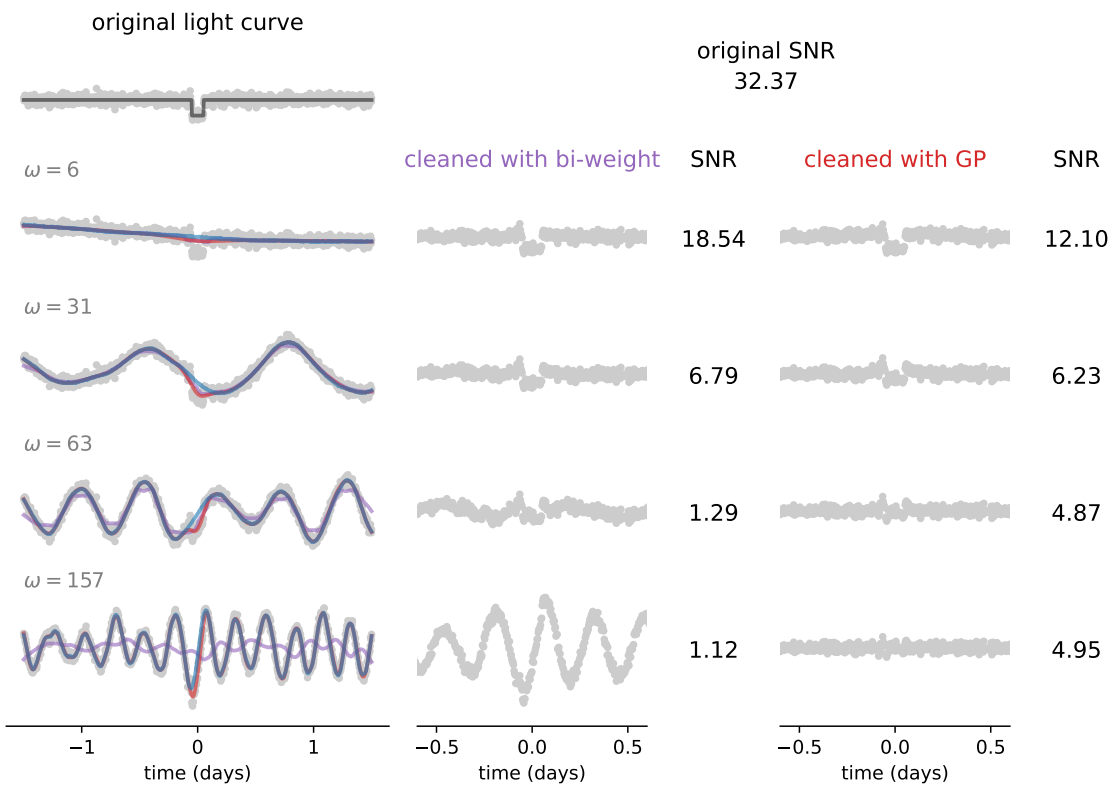

Figure 3. In each plot on the left, correlated noises simulated using a GP with an SHO kernel are added (blue line) to an original light curve containing a transit of depth $\Delta = 0.08$, duration 0.1 day, and white noise with a standard deviation of 0.015 (top left). The hyperparameters of the kernel are fixed to $Q = 10$ and $\sigma = 0.008$, with the pulsation ω increasing from top to bottom. The resulting stellar variability signals are then reconstructed using (in purple) Tukey's bi-weight filter with an optimal window size of $3 \times D$ (see Hippke et al. 2019), and (in red) a GP with the same kernel used to simulate the data. In each case the variability is reconstructed, subtracted, and the transit SNR computed using Equation 2.

To explore the parameter space for which detrending is the most problematic, we employ the model described in Appendix A to simulate 10 000 differential light curves with different morphological characteristics, and compute the remaining transit SNR after detrending. In order to place the stellar variability hyperparameters on a relative scale with the transit signal parameters, we reparametrize the GP kernel with

$$\tau = \frac{\pi}{\omega D}, \quad \delta = \frac{2\sigma}{\Delta} \quad \text{and} \quad Q = 10, \tag{3}$$

where τ is the relative timescale of the variability with respect to the transit duration and δ the relative amplitude of the variability against the transit depth, both being adimensional. Hence, for $(\tau, \delta) = (1, 1)$, the expressions of ω and σ given in Equation 3 correspond to a variability signal with a period half that of the transit duration, and a correlated noise amplitude comparable to the transit depth, i.e. strongly resembling the simulated transit signal.

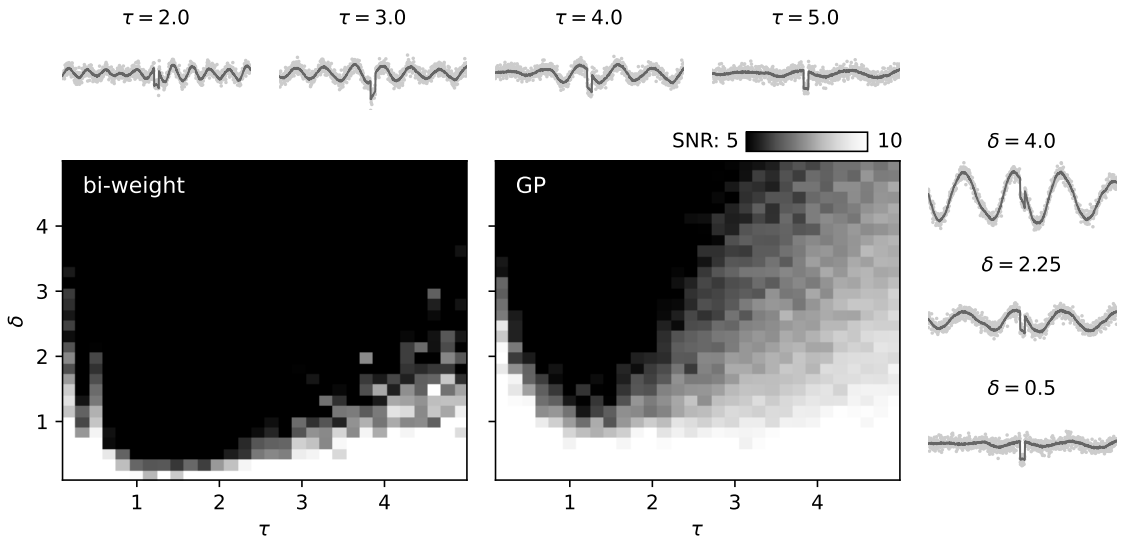

Figure 4. Transit SNR computed for 10 000 differential light curves with varying morphological characteristics. All light curves span 2.8 days with an exposure time of 2 minutes and contain the same transit signal of duration $D = 1$ hour, depth of 0.005 and white noise with a standard deviation of 0.001. Light curves at the top and right side of the central plot are shown with their corresponding τ and δ values, which again correspond to the relative timescale of stellar variability against the transit duration, and the relative amplitude of stellar variability against the transit depth. The two central plots show the transit SNR after detrending the light curves with one of two methods. On the left, light curves are detrended using Tukey's bi-weight filter with an optimal window size of $3 \times D$ (see Hippke et al. 2019), while on the right, light curves are detrended using a GP with the same kernel used to simulate the data.

For each light curve, we separately reconstruct and detrend the variability signal using the two techniques employed in Figure 3, i.e. one using an optimal bi-weight filter with a window size three times that of the transit duration (Hippke et al. 2019) and the other using a GP with an optimal kernel. We then compute the detrended transit SNR using Equation 2.

Figure 4 shows that it exists an entire region of the (τ, δ) parameter space for which the bi-weight detrending degrades transit SNR to the point of no detection ($SNR < 5$). Although being more robust, the same effect is observed when detrending with an optimal GP. Hence, detrending makes transit search blind to many systems, especially when the widely adopted bi-weight filter is used. While this study should be extended to other detrending techniques, it highlights the need for a more informed transit search algorithm able to deal with correlated noise, at least if present in the form of stellar variability.

2. NUANCE

In this section, we present *nuance*, an algorithm capable of searching for planetary transits in light curves containing correlated noise such as instrumental signals and photometric stellar variability.

When searching for exoplanets using an indirect method, such as using transits or radial velocities, the initial detection is often as important as the follow-up observations, ultimately leading to the confirmation of the planetary candidate. For that reason, the final product of most transit search algorithms consists in a *periodogram*: a 1D detection metric given a set of trial periods that enables to identify the presence of a potential candidate, and the period and epoch at which it should be followed up.

If we assume that a transit is defined by its period P, epoch T, duration D and depth Δ, we then wish to compute the likelihood of such a transit being present in the for a set of periods P, leading to an interpretable periodogram. As we are interested in following up transits with specific parameters, such as a well-defined epoch, the likelihood we wish to compute must not be marginalized over all parameters other than P but rather specifically computed at the maximum-likelihood parameters $\hat{T}$, $\hat{D}$ and $\hat{\Delta}$, leading to the *profile likelihood*

$$p(\boldsymbol{f}|P, \hat{T}, \hat{D}, \hat{\Delta}), \tag{4}$$

where $\boldsymbol{f}$ is the data. As in section 1.1 let assume that $\boldsymbol{f}$ is a vector of size N containing the flux of a star observed at times $\boldsymbol{t}$ such that

$$\boldsymbol{f} \sim \mathcal{N}(\boldsymbol{X}\boldsymbol{w}, \boldsymbol{\Sigma}),$$

i.e. that $\boldsymbol{f}$ is drawn from a GP of mean $\boldsymbol{X}\boldsymbol{w}$ and covariance $\boldsymbol{\Sigma}$. Again, the first $M-1$ columns of the $(N \times M)$ design matrix $\boldsymbol{X}$ are contemporaneous instrumental time series measurements and its last column consists in a normalized box-shaped transit of period P, epoch T and duration D. This way, the transit signal is part of the linear model and its depth Δ can be solved linearly. Under this assumption, the log-likelihood of the data given the presence of a periodic transit signal of period P, epoch T and duration D is (Rasmussen & Williams 2005)

$$\ln p(\boldsymbol{f}|P, T, D, \Delta) = -\frac{1}{2}(\boldsymbol{f} - \boldsymbol{X}\boldsymbol{w})^T\boldsymbol{\Sigma}^{-1}(\boldsymbol{f} - \boldsymbol{X}\boldsymbol{w}) - \frac{1}{2}\ln|\boldsymbol{\Sigma}| - \frac{N}{2}\ln 2\pi. \tag{5}$$

In this expression, the vector of parameters $\boldsymbol{w}$ and their errors $\boldsymbol{\sigma}$ are computed using the generalized least-square solution

$$\boldsymbol{w} = (\boldsymbol{X}^T\boldsymbol{\Sigma}^{-1}\boldsymbol{X})^{-1}\boldsymbol{X}^T\boldsymbol{\Sigma}^{-1}\boldsymbol{f} \quad \text{and} \quad \boldsymbol{\sigma} = (\boldsymbol{X}^T\boldsymbol{\Sigma}^{-1}\boldsymbol{X})^{-1}, \tag{6}$$

so that the depth of the transit corresponds to $\hat{\Delta} = \boldsymbol{w}_M$.

Hence, given a period P, computing $Q(P)$ boils down to a non-linear optimization involving several evaluations of the likelihood given in Equation 5. While this is tractable for few periods, it becomes highly intractable for the large set of trial periods required to properly sample a transit search periodogram.

To be tractable, *nuance* employs the strategy of Foreman-Mackey et al. (2015), separating the transit search into two components: the linear search and the periodic search. During the linear search, the likelihood of a single non-periodic transit is computed for a grid of epochs and durations, requiring the evaluation of $p(\boldsymbol{f}|T, D)$ for a fixed number of times. Then, the periodic search consists in combining these likelihoods to compute the likelihood $p(\boldsymbol{f}|P, T, D)$ of the data given a periodic transit signal for a range of periods P. These combined likelihoods yield a transit-search periodogram on which the periodic transit detection is based. `nuance` differs from Foreman-Mackey et al. (2015) and other existing transit search algorithms as it models the covariance of the light curve with a GP, accounting for correlated noise (especially in the form of stellar variability) while keeping the model linear and tractable. This way, `nuance` searches for transits while, at the same time, modeling correlated noise, avoiding the detrending step that degrades transit signals SNR (see section 1).

We note that the approach employed by *nuance* (using the two steps proposed by Foreman-Mackey et al. 2015), shares similarities with the approach of Jenkins et al. (2010), where a single event statistic is computed and combined into a multiple event statistics.

2.1. *The linear search*

The goal of the linear search is to compute the likelihood $p(\boldsymbol{f}|T, D)$ for a grid of epochs $\{ T_i \}_i$ and durations $\{ D_j \}_j$. For each pair (T_i, D_j) the transit depth $\Delta_{i,j}$ is linearly solved and follow a Gaussian distribution of mean $\hat{\Delta}_{i,j}$ and standard deviation $\sigma_{i,j}$, computed using Equation 6. Hence, the linear search lead to the set of maximum-likelihoods

$$\{ \ln \mathcal{L}_{i,j} \}_{i,j} = \{ \ln p(\boldsymbol{f}|T_i, D_j, \hat{\Delta}_{i,j}) \}_{i,j}.$$

An example of such a grid of likelihoods is shown in Figure 5.

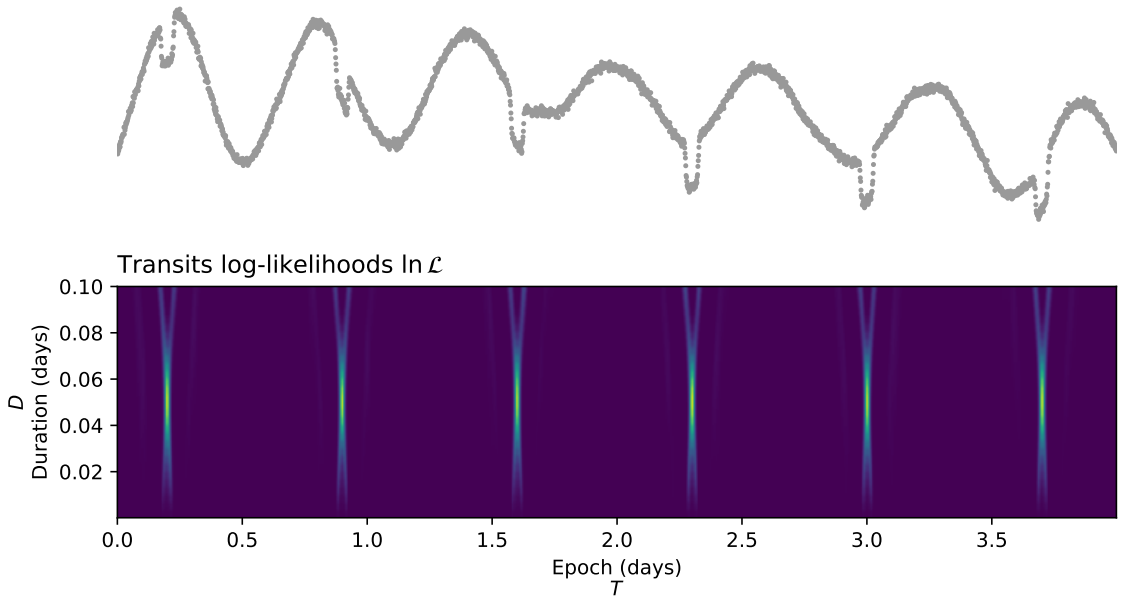

Figure 5. Principle and output of the linear search. The simulated dataset (top) corresponds to the one shown and described in Figure 18. First, a set of durations and depths $\{ T_i, D_j \}_{i,j}$ is generated. For each pair of indices (i, j), the likelihood $\ln p(\boldsymbol{f}|T_i, D_j, \Delta_{i,j})$ is computed using the parameters from Equation 6 and the expression of Equation 5. This process yields the grid of log-likelihoods $\ln \mathcal{L}$ (bottom plot), as well as the $\{ \Delta_{i,j}, \sigma_{i,j} \}_{i,j}$ transit depths and errors inferred linearly using Equation 6.

To prepare for the next step, the corresponding depths $\Delta_{i,j}$ linearly solved for any (T_i, D_j) are stored, as well as their associated uncertainties $\sigma_{i,j}$, corresponding to

$$\Delta_{i,j} = \boldsymbol{w}_M \quad \text{and} \quad \sigma_{i,j} = \boldsymbol{\sigma}_{MM},$$

M denoting the index of the last column of the design matrix $\boldsymbol{X}$, where the transit signal is contained.

2.2. *The periodic search*

We then need to combine the likelihoods computed from the *linear search* to obtain

$$p(\boldsymbol{f}|P, T, D, \Delta),$$

i.e. the probability of a periodic transit of period P, epoch T_0, duration D and depth Δ given the data $\boldsymbol{f}$. For a given transit duration D, any combination of (P, T) leads to K transits, for which it is tempting to write

$$p(\boldsymbol{f}|P, T, D, \Delta) = \prod_k^K p(\boldsymbol{f}|T_k, D, \Delta_k), \tag{7}$$

where $\{ T_k \}_k$ are the epochs matching (T_0, P) and $\{ \Delta_k \}_k$ the corresponding depths. So that

$$\ln p(\boldsymbol{f}|P, T, D, \Delta) = \sum_k^K \ln \mathcal{L}_k.$$

This is the joint likelihood of transits belonging to the same periodic signal but with varying depths $\{\,\Delta_k\,\}_k$. However, individual transits from a periodic signal cannot be considered independent, and should instead be found periodically and share a common transit depth Δ. To this end, it can be shown (see Appendix B) that there is an analytical expression for the joint likelihood of K individual transits with depths and errors $\{\,\Delta_k, \sigma_k\,\}_k$ assuming a common depth Δ, corresponding to

$$\ln p(\boldsymbol{f}|P, T_0, D, \Delta) = \sum_k^K \ln \mathcal{L}_k - \frac{1}{2}\sum_k^K \left(\ln(\sigma_k^2) - \ln(\sigma^2 + \sigma_k^2) + \frac{(\Delta_k - \Delta)^2}{\sigma_k^2 + \sigma^2} \right)$$
$$\text{with} \quad \frac{1}{\sigma^2} = \sum_k^K \frac{1}{\sigma_k^2} \quad \text{and} \quad \Delta = \sigma^2 \sum_k^K \frac{\Delta_k}{\sigma_k^2}. \tag{8}$$

While Equation 8 takes a closed form, the individual epochs matching T_0 and P are not necessarily available in the grid of epochs $\{\,T_k\,\}_k$. In Foreman-Mackey et al. (2015), a similar issue is solved by using the nearest neighbors in the epochs grid. Instead, to allow the efficient matrix computation of Equation 8, the likelihood grid is linearly interpolated from $\{\,T_i\,\}_i$ to a common grid of transit phases $\{\,\phi_i\,\}_i$, leading to the periodic search log-likelihood

$$\ln \mathcal{P}(P) = \{\,\ln p(\boldsymbol{f}|P, \phi, D)\,\}_{i,j}$$

shown for few periods in Figure 6 (b). In the latter equation, $\Delta_{i,j}$ is omitted since being interpolated from the linear search using ϕ_i, D_j and $T_0 = 0$.

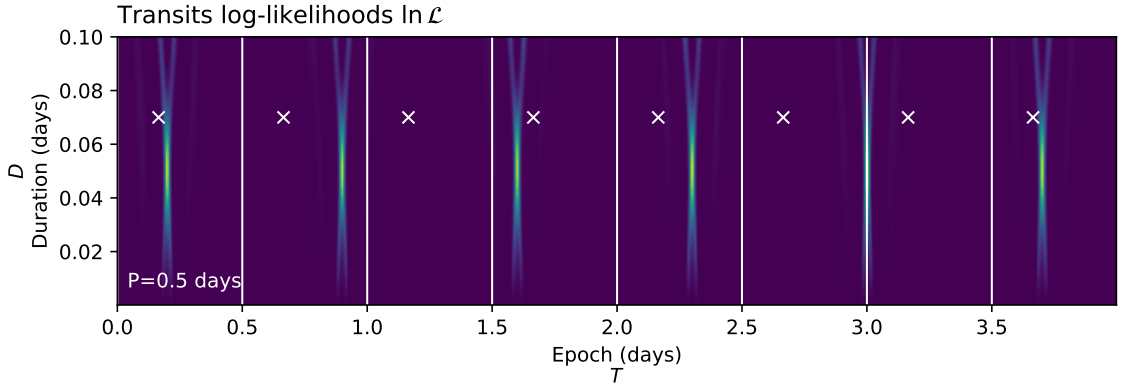

(a) $\ln \mathcal{L}$

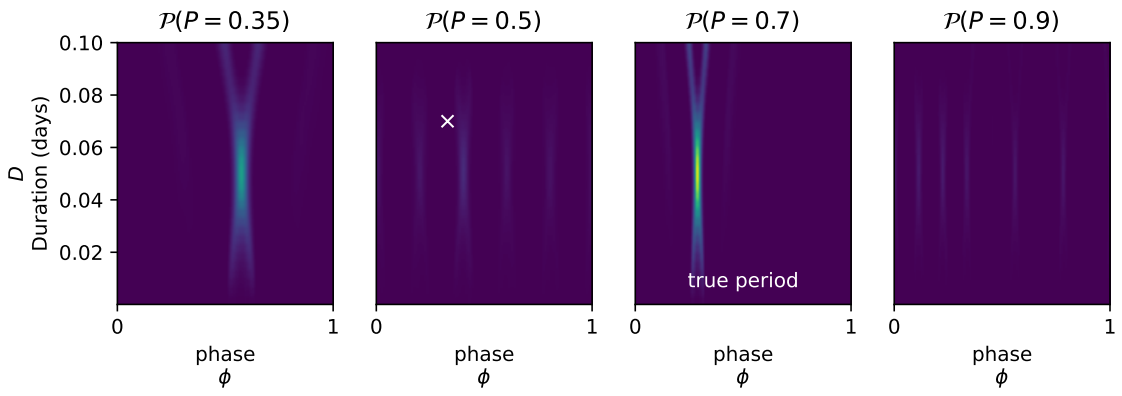

(b) $\mathcal{P}(P)$

Figure 6. Applied to the dataset shown in Figure 5, this figure shows how the periodic search works at different periods P (including the true period $P = 0.7$ days). Given different periods P and $T_0 = 0$, the likelihood $\ln \mathcal{L}$ shown in (a) is phase-folded and interpolated onto a common grid of phases shown in (b). As an example, the white lines in (a) mark the edges of each fold for a period $P = 0.5$ days, and the white crosses show the epochs $\{ T_k \}_{k \in \mathbb{K}}$ matching a particular phase in the grid (reported in (a) and (b)) on which the corresponding $\{ \ln \mathcal{L}_k \}_{k \in \mathbb{K}}$ are interpolated and combined using Equation 8. To allow the use of efficient matrix computations, this is done for all durations $\{ D_i \}_i$ so that $\mathcal{P}$ is computed on the full grid $\{ D_i, \phi_i \}_{i,j}$ at once. We understand from the folded likelihoods plots in (b) that a different choice of epoch T_0 may only shift the results in phase but do not affect the values of $\mathcal{P}$. For this reason, computing $\mathcal{P}$ for $T_0 = 0$ is sufficient. We also notice how the maximum value of $\mathcal{P}(P = 0.7/2)$ (left plot of (b)) is lower than for $P = 0.7$ days, a result of combining the log-likelihoods using Equation 8 instead of Equation 7, in favor of individual transits matching a common depth Δ.

2.3. *The transit search periodogram*

Using Equation 8, we can now compute $\ln \mathcal{P}$ for a range of periods and build a transit search periodogram using Equation 4. But a final issue emerges, one that is fundamentally linked to our strategy. Each likelihood $p(\boldsymbol{f}|T, D, \Delta)$ estimated during the linear search is computed using N measurements. Hence, combining transits in the periodic search, through Δ_k, σ_k and the product of K likelihoods $\{ \mathcal{L}_k \}_k$ (see Equation 8), artificially leads to a likelihood involving $N \times K$ measurements. This lead to a normalization issue when trying to compare the joint log-likelihoods $\mathcal{P}(P)$ from one period to another, as the number of observed transits differs from one period to another. This motivates a final step to produce the transit search periodogram $\mathcal{Q}$. For any period P, instead of taking $\mathcal{Q}(P)$ as the maximum value of $\ln \mathcal{P}$, we compute the maximum likelihood parameters

$$(\phi_0, D) = \underset{\phi_i, D_j}{\arg\max} \{ \ln p(\boldsymbol{f}|P, \phi_i, D_j) \}_{i,j} \tag{9}$$

and defined $\mathcal{Q}(P)$ as being equal to the SNR of the transit of period P, epoch $T_0 = \phi_0 P$, duration D and depth Δ, i.e.

$$\mathcal{Q}(P) = \frac{\Delta}{\sigma},$$

where Δ and σ are obtained using Equation B6 with the last column of X containing a periodic transit signal of period P, epoch T_0, duration D and depth 1. This process and the resulting periodogram $\mathcal{Q}$ are shown in Figure 7.

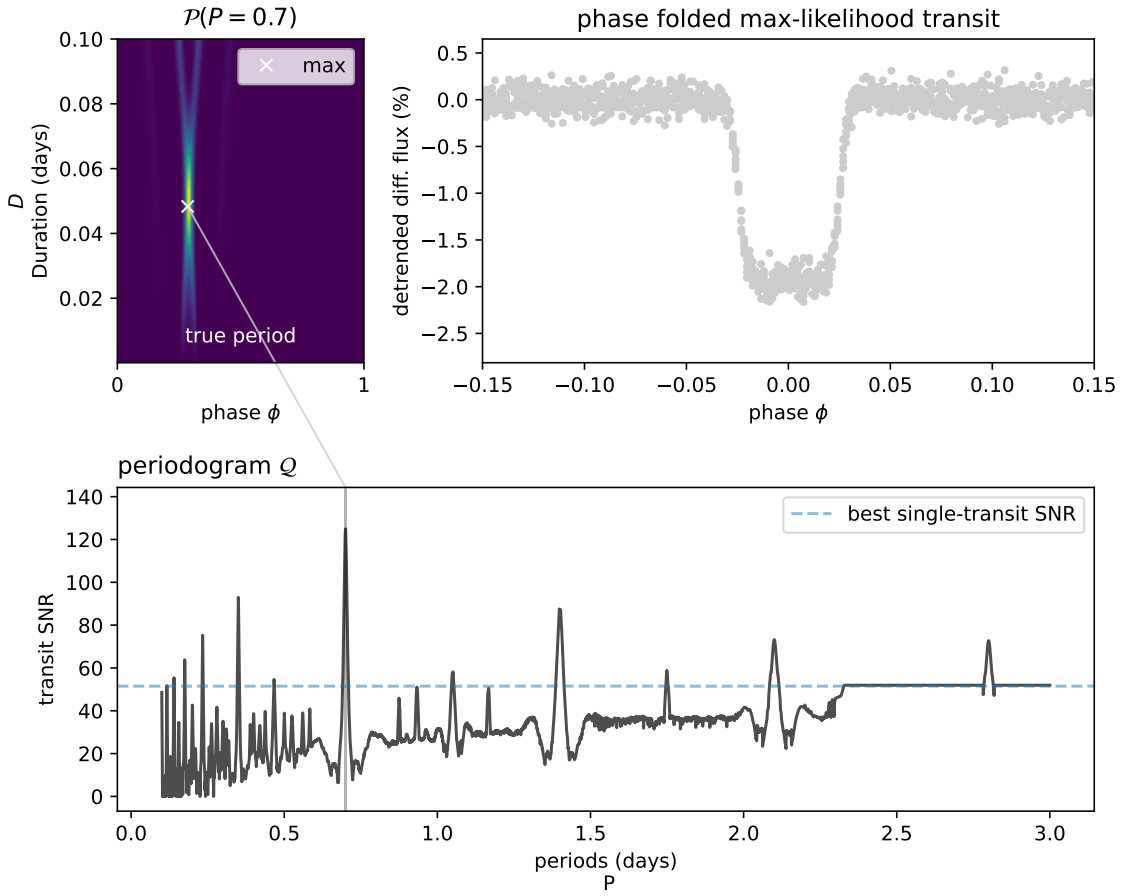

Figure 7. For each period P, the joint likelihood $\mathcal{P}(P)$ is computed using Equation 8, and the value of the maximum likelihood transit SNR retained as $\mathcal{Q}(P)$.

The periodic transit of period P with the maximum SNR, i.e. maximizing $\mathcal{Q}$, is adopted as the best candidate, basing the confidence in this signal through its SNR. The parameters of this transit are the period P, the epoch $T_0 = \phi_0 P$ and duration D (Equation 9), and the depth Δ with error σ (given by Equation 8).

2.4. *An open-source python package*

Methods presented in this paper are made accessible through the nuance open-source Python package, hosted on Github[3] and released on the Python Package Index[4].

To instantiate a search, a user can start by creating a Nuance object with

[3] https://github.com/lgrcia/nuance
[4] https://pypi.org/project/nuance/

```
from nuance import Nuance

nu = Nuance(time, flux, gp=gp, X=X)
```

where gp is a tinygp GP instance and X the design matrix of the linear model. nuance exploits the use of tinygp[5], a Python package powered by JAX[6], allowing for custom kernels to be built and highly tractable computations. We can then define a set of epochs t0s and durations Ds and run the linear search with

```
import numpy as np

t0s = time.copy()
# a range of 10 durations
Ds = np.linspace(0.01, 0.2, 10)
nu.linear_search(t0s, Ds)
```

Finally, the periodic search is run with

```
# range of periods
periods = np.linspace(0.1, 5, 2000)
search = nu.periodic_search(periods)
```

From this `search` object, the best transiting candidate parameters can be computed (search.best), or the $\mathcal{Q}$ periodogram retrieved (search.Q_snr), together with valuable information about the transit search. The Nuance object also provides methods to perform transit search on light curves from multi-planetary hosts, the advantage of *nuance* being that the linear search only needs to be performed ones and reused for the search of several transiting candidates (cf. section 3.3). An extensive and maintained online documentation is provided at `nuance.readthedocs.io`.

2.5. *Comparison with BLS*

To start testing *nuance* against existing methods, a simple adimensional normalized light curve is simulated, consisting in pure white noise with a standard deviation of 5×10^{-4} spanning 6 days with an exposure time of 2 minutes. From this signal, we produce 4000 light curves, each containing box-shaped transits with periods randomly sampled from 0.3 to 2.5 days, durations of 50 minutes, and depths randomly sampled to lead to transit SNRs ranging from 4 to 30. For each light curve, transits are searched using two different tools: nuance, using its implementation from the Python package described in the previous section; and BLS, the Box-Least-Square algorithm from Kovács et al. (2002) (using astropy's BoxLeastSquares[7] implementation).

[5] https://github.com/dfm/tinygp
[6] https://github.com/google/jax
[7] https://docs.astropy.org/en/stable/api/astropy.timeseries.BoxLeastSquares.html

For both methods, 3000 trial periods from 0.2 to 2.6 days are searched, with a single trial duration fixed to the unique known duration of 50 minutes. A transit signal is considered detected if the absolute difference between the injected and the recovered period is less than 0.01 day. To ease the detection criteria, orbital periods recovered at half or twice the injected ones (aka *aliases*) are considered as being detected. For this reason, detected transit epochs are not considered (although manually vetted). Results from this *injection-recovery* procedure are shown in Figure 8.

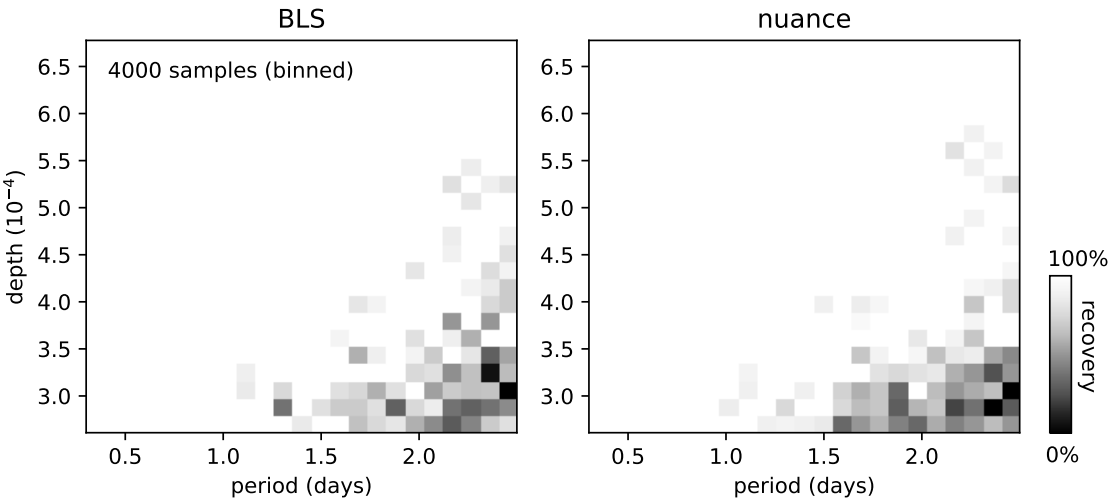

Figure 8. Binned statistics of the injection-recovery of 4000 transit signals in a flat light curve with only white noise using BLS and nuance. The color scale indicates the recovery of transits in the corresponding (period, depth) parameter space, white for a full recovery and black for no detection.

These results demonstrate the qualitative match between the detection capabilities of nuance and BLS on light curves with no correlated noise. Explaining the subtle differences observed between the two methods when only white noise is present is beyond the scope of this paper, and we will assume that any differences observed in the following sections are due to the different treatments of correlated noise.

3. PERFORMANCES

3.1. *Comparison with `biweight+BLS` on simulated light curves*

Figure 4 shows that nuance's full-fledged modeling capabilities may not always be necessary and may only be beneficial for certain noise characteristics, relative to the searched transit parameters. Here, we evaluate the performance of nuance in the relative parameter space (τ, δ) described in Equation 3 and see when its specific treatment of correlated noise in the transit search becomes necessary.

We compare nuance to the approach that involves removing stellar variability from light curves before performing the search on a detrended dataset. Similarly to section 1.3, an optimal bi-weight filter implemented in the wõtan Python package[8] is used with a window size three times that of the injected transit duration. A transit search on the detrended light curve is then performed using the BLS algorithm, like in section 2.5 using the astropy BoxLeastSquares implementation[9]; a strategy commonly used in the literature that we denote `biweight+BLS`. In what follows, the transit detection criteria are the same as the ones used in section 2.5, i.e. that a transit is considered recovered if the absolute difference between the injected and recovered period is less than 0.01 days, including periods found at half or twice the injected ones (aliases) and ignoring the value of the recovered transit epoch.

DATASET

The dataset consists in 4000 light curves simulated using the model fully described in Appendix A. We simulate a common periodic transit added to all light curves, of period $P = 1.1$ days, epoch $T_0 = 0.2$ days, duration $D = 0.04$ days and depth $\Delta = 1\%$. Each light curve consists in a 4 days observation with an exposure time of 2 minutes, leading to $N = 2880$ data points with a normal error of 0.1%. As in section 2.5, only box-shaped transits are injected, using the model from Protopapas et al. (2005) with $c = 500$ (cf. section A.1).

For a given pair of (τ, δ), we simulate stellar variability using a GP with an SHO kernel of hyperparameters defined by Equation 3 (except for Q, described below), computed with respect to the injected transit parameters D and Δ. The same kernel is used for the search with nuance, an optimal choice on equal footing with the optimal $3 \times D$ window size of the bi-weight filter employed in the `biweight+BLS` search. 4000 pairs of (τ, δ) are generated such that

$$\tau \sim \mathcal{U}(0.1, 10), \quad \delta \sim \mathcal{U}(0.1, 25) \quad \text{and} \quad Q \sim \mathcal{U}(10, 100)$$

where $\mathcal{U}(a, b)$ denotes a uniform distribution of lower bound a and upper bound b.

[8] https://github.com/hippke/wotan
[9] https://docs.astropy.org/en/stable/api/astropy.timeseries.BoxLeastSquares.html

The results of this injection-recovery procedure are shown in Figure 9 and highlight particularly well the benefit of `nuance` against the `biweight+BLS` strategy on transits with relatively large depth compared to the stellar variability amplitude, and a relatively large duration compared to the stellar variability period. This empirical statement only concerns light curves with a given amount of white noise, and may vary depending on the length of the observing window or the number of transits. For this reason, quantifying for which values of (τ, δ) `nuance` outperforms `biweight+BLS` would only apply to this specific but representative example. However, we verify that our conclusions remain qualitatively valid for various simulation setups.

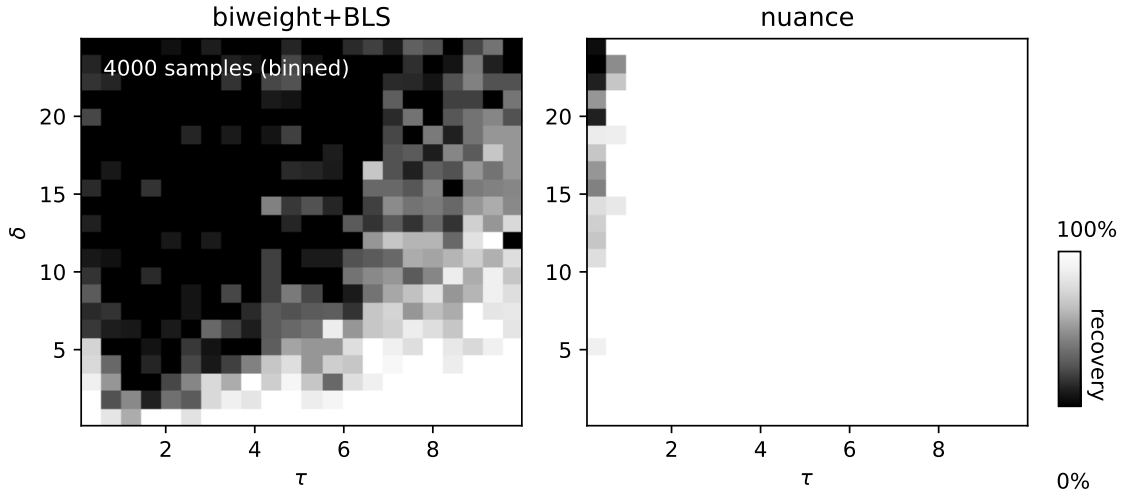

Figure 9. Injection-recovery results on 4000 simulated light curves described in section 3.1. The color scale represents the fraction of recovered transits, white if all injected transits are recovered in a given portion of the (τ, δ) parameter space, black if none are recovered.

This injection-recovery is done in a particularly optimal setup, on light curves not all physically realistic and using an optimal GP kernel, hence demonstrating the performance of `nuance` only on a purely experimental basis. In the next section, we perform transits injection-recovery on real space-based light curves.

3.2. *Comparison with various techniques on rapidly-rotating M dwarfs TESS light curves*

In order to assess the performance of *nuance* on real datasets, we inject and recover transits into light curves from the Transiting Exoplanet Survey Satellite (TESS, Ricker et al. 2015). The goal of this transit injection-recovery is to compare *nuance* to other transit search strategies, and to understand the light curves characteristics for which it becomes beneficial.

We focus this proof of concept on light curves from a list of 438 M-dwarfs found to have detectable rotation signals with periods lower than one day (Ramsay et al. 2020), which lead to a parameter space justifying the use of *nuance*. For each of the studied target, transits are injected and recovered in the TESS 2 min cadence SPOC Simple Aperture Photometry and Pre-search Data Conditioning light curves (PDCSAP, Caldwell et al. 2020) of a single sector (the first being observed for each target) spanning on average 10 days.

In this injection-recovery tests, *nuance* is compared to other transit search strategies employing the BLS algorithm, for each of them after detrending the light curves with a different technique:

- `bspline+BLS` employs a B-spline[10] for detrending, fitted using the scipy.interpolate.splrep function[11], followed by a search with the BLS algorithm.
- `biweight+BLS` employs an optimal bi-weight filter implemented in the wõtan Python package (Hippke et al. 2019) with an optimal window size of $3 \times D$ (i.e. three times the transit duration), followed by a search with the BLS algorithm.
- `harmonics+BLS` employs a linear harmonic detrending, where the light curve is modeled as a Fourier series including four harmonics of the stellar rotation period found by Ramsay et al. (2020), with coefficients found through ordinary least square. This detrending is followed by a search with the BLS algorithm.
- `iterative+BLS` iteratively detrends the light curve with a sinusoidal signal fitted to the data, each time using the dominant period of the residuals found using a lomb-scargle periodogram (5 iterations). This detrending is followed by a search with the BLS algorithm.

LIGHT CURVE CLEANING AND TRANSITS INJECTION

As some of the techniques compare to *nuance* can be affected by gaps in the data, we only use continuous measurements from half a TESS sector. We assume that all

[10] https://docs.scipy.org/doc/scipy/reference/generated/scipy.interpolate.BSpline.html
[11] https://docs.scipy.org/doc/scipy/reference/generated/scipy.interpolate.splrep.html

methods (including *nuance*) are based on an incomplete model of the data that do not account for stellar flares. For this reason, the light curve of each target is cleaned using an iterative sigma clipping approach. For each iteration, points 3 times above the standard deviation of the full light curve (previously subtracted by its median) are identified. Then, the 30 adjacent points on each side of the found outliers are masked. This way, large flare signals and their expected ingress and egress are masked, using a total of 3 iterations. At each iteration, the GP kernel hyperparameters are re-optimized. As PDCSAP light curves often start with a ramp-like signal, the first 300 points (as well as the last 300 points) of each continuous observation are masked. Finally, each light curve is normalized by its median value. Such a cleaned light curve is shown in Figure 10. We note that the gaps left after sigma clipping may be problematic for some of the detrending techniques (such as `bspline+BLS`). However, adopting this flare cleaning step and analyzing light curves with few small gaps is a practice commonly found in the literature.

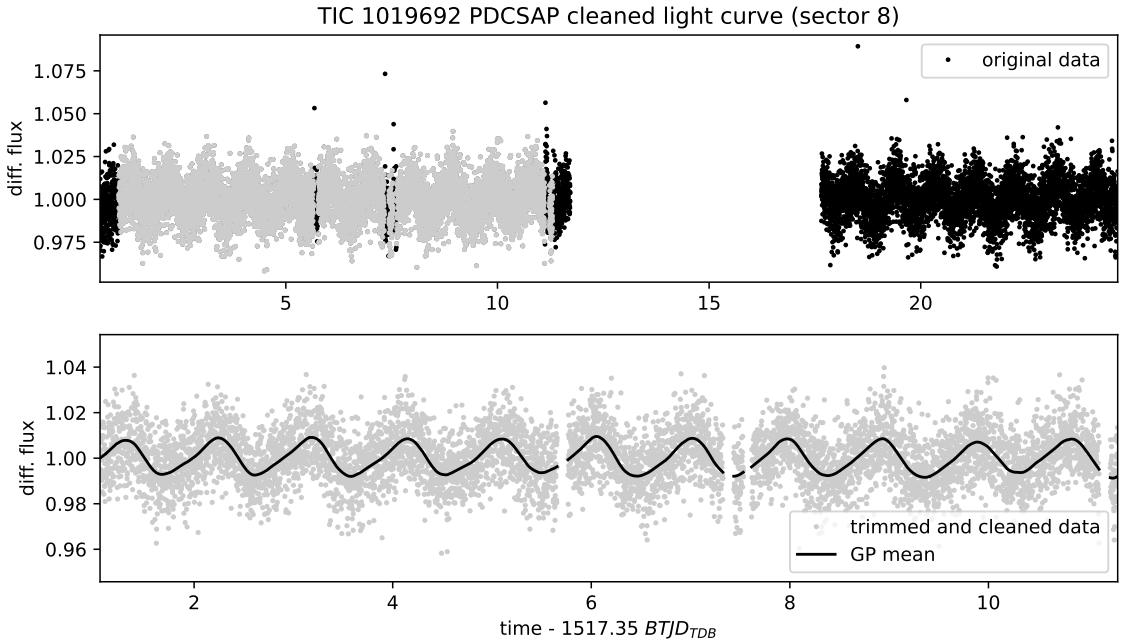

Figure 10. Trimmed and cleaned single-sector light curve of the target TIC 1019692. Top plot shows how much of the data is truncated and sigma clipped, resulting in a quasi-continuous light curve shown in the bottom plot. On this bottom plot, the black line corresponds to the mean of the GP model (with hyperparameters optimized here on the cleaned light curve).

For each light curve, transits of planets with 10 different orbital periods combined with 10 planetary radii are individually considered, for a total of 100 periodic transits injection-recovery per target. Orbital periods P are sampled on a regular grid between 0.4 and 5 days, and planetary radii R_p are sampled on a regular grid designed to yield a minimum transit SNR of 2 and a maximum of 30. Using Equation 2 with $\sigma_r = 0$,

the planetary radius leading to a transit with a desired SNR s is given by

$$R_p = R_\star \, n^{-\frac{1}{4}} \sqrt{\sigma s}$$

with σ equal to the mean uncertainty estimated by the SPOC pipeline, $R_\star$ the radius of the star reported by Ramsay et al. (2020) and n the number of points in transit computed using a transit duration assuming a circular orbit.

STELLAR VARIABILITY KERNEL

One of the particularity of *nuance* is to model a light curve as a GP. To model these TESS light curves, we employ a mixture of two SHO kernels of period $P_\star$ and $P_\star/2$ (with $P_\star$ the rotation period of the star), a model representative of a wide range of stochastic variability in stellar time series[12]. In order to account for additional correlated noises, we complement this kernel with a short and a long-timescale exponential term, so that the full kernel can be expressed as

$$k = k_1 + k_2 + k_3 + k_4$$

with

- k_1 a SHO kernel with hyperparameters

$$Q_1 = 1/2 + Q_0 + \delta Q\,, \quad \omega_1 = \frac{4\,\pi\,Q_1}{P\,\sqrt{4\,Q_1^2 - 1}} \quad \text{and} \quad S_1 = \frac{\sigma^2}{(1+f)\,\omega_1\,Q_1}.$$

- k_2 a SHO kernel with hyperparameters

$$Q_2 = 1/2 + Q_0\,, \quad \omega_2 = 2\omega_1 \quad \text{and} \quad S_2 = \frac{f\,\sigma^2}{(1+f)\,\omega_2\,Q_2},$$

where Q_0 is the quality factor for the secondary oscillation, δQ is the difference between the quality factors of the first and the second modes, f is the fractional amplitude of the secondary mode compared to the primary and σ is the standard deviation of the process. The kernels k_3 and k_4 are expressed as

$$k(t, t') = \sigma^2 \, \exp\left(-\frac{|t - t'|}{\ell}\right),$$

with ℓ and σ the scale and standard deviation of the process. These are meant to model short and long-timescale non-periodic correlated noise. In total, the rotation kernel k has 8 hyperparameters.

[12] https://celerite2.readthedocs.io/en/latest/api/python

The hyperparameters of this kernel are optimized on trimmed and cleaned light curves containing the injected transits, using the scipy.optimize.minimize[13] wrapper provided by the jaxopt Python package, and taking advantage of the JAX implementation of tinygp and its quasiseparable kernels[14] (Foreman-Mackey et al. 2017). As correlated noise is expected to affect the light curve uncertainty estimates performed by SPOC, the diagonal of the full covariance matrix of the data (i.e. their uncertainty, assuming homoscedasticity) is held free, increasing the number of optimized parameters to 9. The optimization is performed using the BFGS algorithm (Fletcher 1987), minimizing the negative log-likelihood of the data as expressed in Equation 5 (without transit), i.e. accounting for a linear systematic model of the data in addition of stellar variability. For simplicity, and to adopt a uniform treatment for all target light curves, a design matrix $\boldsymbol{X}$ with a single constant column is adopted, such that the systematic model only consists in a single parameter corresponding to the mean value of the differential flux (expected to be close to 1) solved linearly. Our motivations to choose this very simplistic baseline, despite the capability of *nuance* to account for more complex linear models, is discussed in section 4.2.

SEARCH PARAMETERS AND TRANSIT DETECTION CRITERIA

For all techniques, we only search for transits with a duration fixed to the known duration of the injected transits. This is mainly done for computational efficiency and allows for a narrower comparison between *nuance* and all BLS-based techniques. Finally, the search is done over 4000 trial periods linearly sampled from 0.3 to 6 days. A realistic transit search on a wider parameter space (e.g. multiple trial durations) is discussed in the next section.

Like in previous sections, we consider the detection of period aliases and ignore the match between the injected and recovered transit epochs (although we visually vet that the found epochs were consistent with the ones injected for cases where the planet was detected). We consider a transit detectable if its original SNR is greater than 6. Hence we define *true positives* has detectable transits recovered with the correct period (or an alias) and a measured SNR greater or equal to 6, and *false positives* as non-detectable transits recovered with a measured SNR greater or equal to 6.

As we noticed that few methods were still affected by the remaining stellar variability after detrending, we remove from the grid of trial periods all periods close to the stellar rotation period and its aliases. In practice this is done by removing all periods P such that $dP = \frac{P}{P_*}$ is less than 2% from an integer value, i.e. $|dP - \lceil dP \rceil| < 0.02$.

[13] https://jax.readthedocs.io/en/latest/_autosummary/jax.scipy.optimize.minimize.html
[14] https://tinygp.readthedocs.io/en/latest/api/kernels.quasisep.html

An example of the transit injection-recovery and its result is shown in Appendix C for the target TIC 1019692. Figure 11 shows the global results of the injection-recovery for all targets, while Figure 12 shows the true and false positives plotted against the relative parameters τ and δ (defined in Equation 3). These figures are a synthesis of Figure 13 that shows the rate of true and false positives binned in the full parameter space (τ, δ).

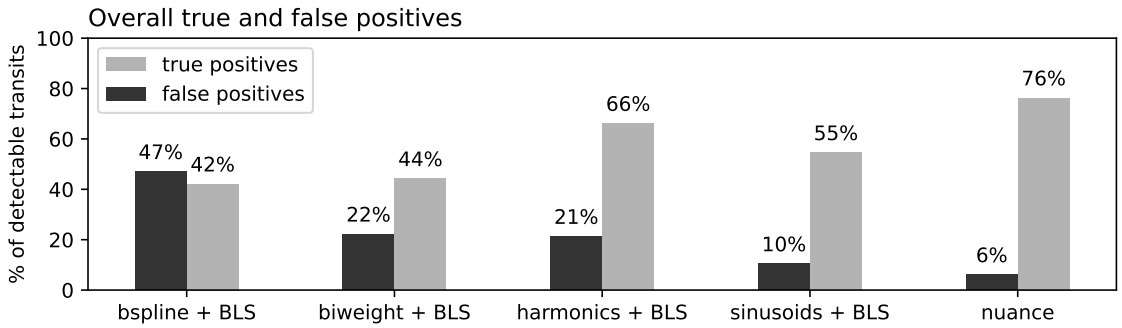

Figure 11. Rate of true and false positives for all methods as a fraction of detectable transit signals.

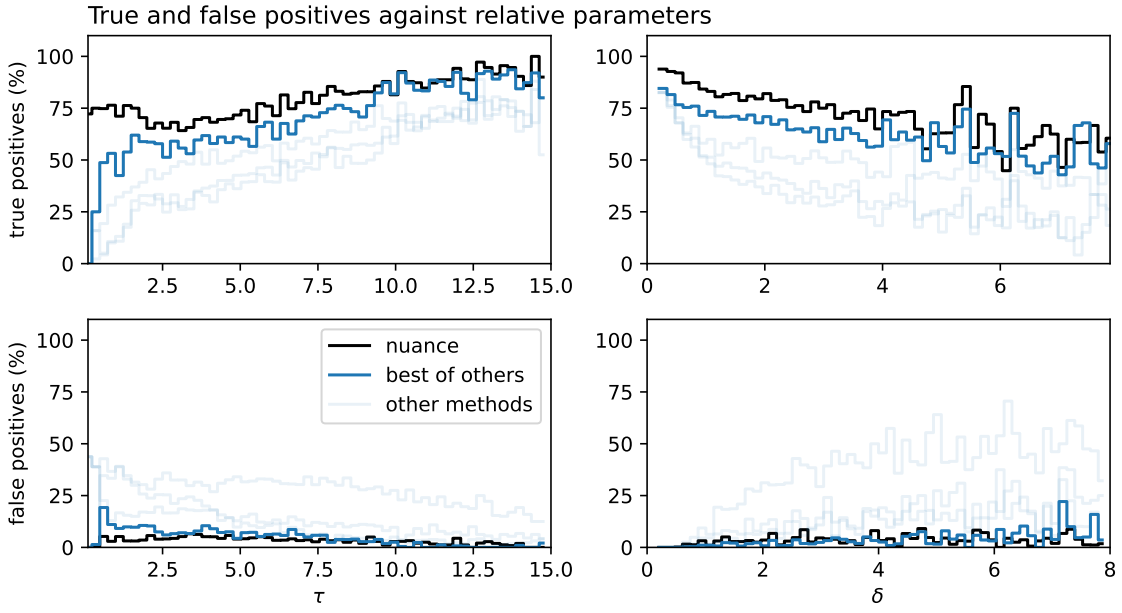

Figure 12. Rate of true and false positives of *nuance* compared to other methods, as a function of the relative parameters τ and δ. The solid red line corresponds to the maximum of true positives among all methods on the top panel, and the minimum of false positives on the bottom panel.

Compared to other techniques, we find that nuance leads to the highest number of true positives, with a successful detection of 76% of the 7008 detectable transits (Figure 11). While the performances of other methods highly depend on the characteristics of the variability, **nuance is the best technique in 93% of cases, leading to both the highest number of true positives and the lowest number of false positives** (Figure 11).

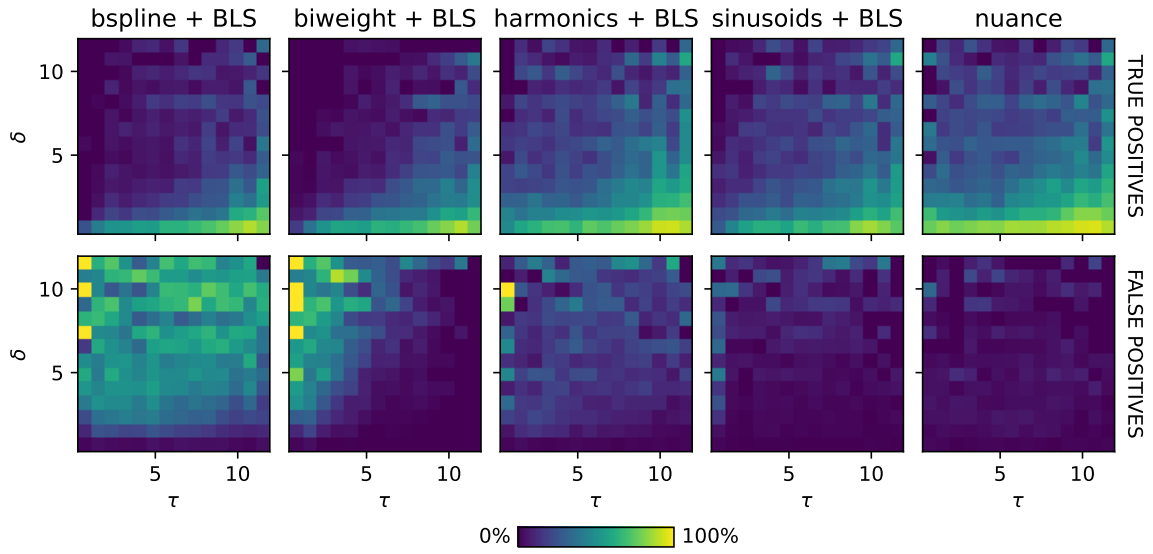

Figure 13. Rate of true and false positives binned over the full parameter space (τ, δ) for all methods.

3.3. *Comparison for a multi-sector TESS candidate: TOI-540*

In order to further validate nuance on a realistic dataset, we focus this section on the multi-sector TESS light curves of TOI-540, and the search for its earth-like companion TOI-540 b (Ment et al. 2021). We download the 2 minutes cadence SPOC PDCSAP light curves of TOI-540 observed in 5 sectors (4, 5, 6, 31 and 32). Like in the previous section, we use a Lomb-Scargle periodogram and identify the 0.72 days rotation period of the star, that we use as an initial value to optimize the kernel described in section 3.2 on each sector independently. Here again, we employ an upper-sigma-clipping to mask flares out of the data. The resulting light curve for sector 4 and its mean model are shown in Figure 14.

For each sector, we perform the linear search of nuance on the cleaned light curve, using the original times as the trial epochs and 10 trial transit durations linearly sampled from 15 minutes to 1.5 hours. We then perform the periodic search on all sectors combined, using a concatenation of all linear searches. By adopting this by-sector GP modeling of the light-curve, the linear search of *nuance* scales linearly with the number of sectors being processed.

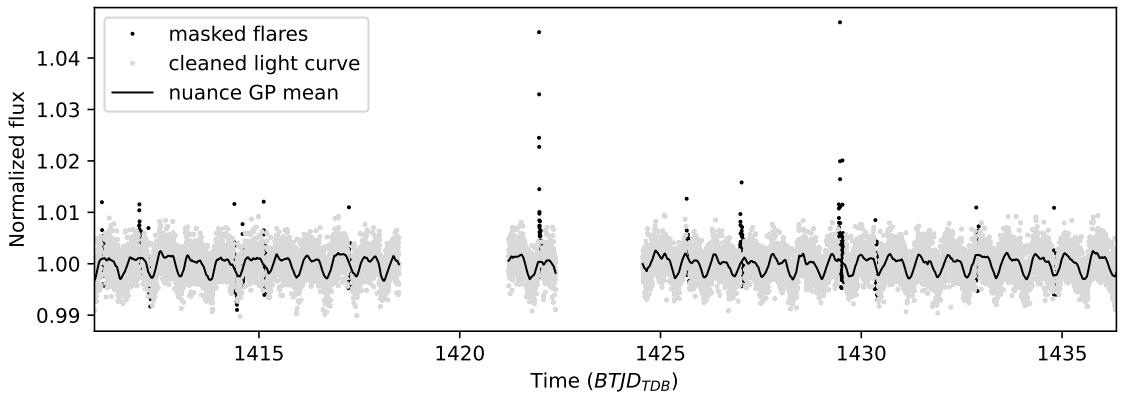

Figure 14. Sector 4 light curve of TOI 540. The cleaned signal (gray points) has been masked for flares (black points), and the black line corresponds to the mean of the GP model.

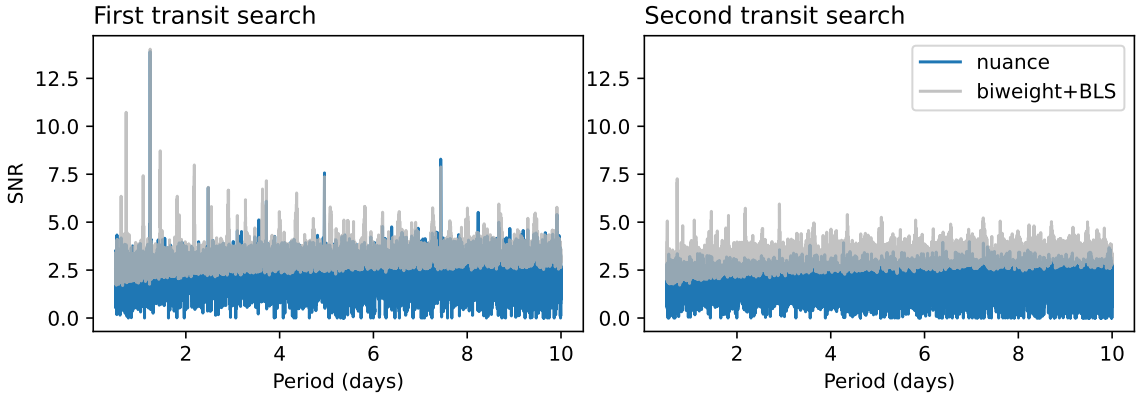

Figure 15. Transit search SNR periodograms of TOI-540 using `biweight+BLS` and *nuance*. After a first periodic search (left panel), the epochs corresponding to the maximum-SNR transit are masked before the second search is performed (right panel).

This approach is adopted for efficiency but also to encapsulate the changing properties of stellar variability from one sector to another, often separated by year-long gaps. The periodic search is done on 20 000 trial periods ranging from 0.5 to 10 days. This search, using `nuance`, is compared to the more traditional approach that consists in detrending each sector with a bi-weight filter and then search for transits with the BLS algorithm (denoted `biweight+BLS` and described in section 3.2) on all sectors combined. Since we don't know the transit duration a-priori, we perform the detrending and BLS search using 15 filtering window sizes sampled from 30 minutes to 5 hours, and retain the search that leads to the highest transit SNR peak in the periodogram (as done e.g. in the SHERLOCK transit search pipeline described in Pozuelos et al. 2020). The results of this comparison are shown in Figure 15.

After a first periodic search, trial epochs in windows of widths $2 \times D$ centered

on the detected periodic transits are masked. In practice, this is done by masking the linear search products $\{ \ln \mathcal{L}_{i,j} \}_{i,j}$, $\{ \Delta_{i,j} \}_{i,j}$ and $\{ \sigma_{i,j} \}_{i,j}$ (defined in section 2.1).

As seen in Figure 15, the SNR periodogram using `biweight+BLS` and `nuance` are very similar, with the known transiting exoplanet TOI-540 b detected with an orbital period P = 1.24 days. This is well expected as the relative parameter τ equal 13 for TOI-540 b [15], which lies outside the range where *nuance* is expected to be beneficial beneficial (see Figure 4). Nonetheless, the *nuance* periodogram of TOI 540 features less spurious SNR peaks, largely due to the penalty naturally occurring when single transits with different depths are periodically combined. In the second search (right panel) of Figure 15, we also notice a higher number of peaks that would lead to false positive detections of transits in the `biweight+BLS` case. The proper treatment of correlated noise in *nuance*, as observed in section 3.2, makes these peaks non-significant, avoiding a large number of false detections.

We note that finding a TESS candidate that displays characteristics for which *nuance* is expected to be significantly beneficial proved to be very challenging during the writing of this paper, as transits with such characteristics are expected to be missed by current state-of-the-art techniques (see e.g. Figure 9). Nontheless, we verify that *nuance* is capable of finding a large number of already known transiting exoplanet candidates, in light curves featuring various forms of correlated noises, at least as efficiently as with commonly used techniques. We reserve the search for new transit signals to a follow-up publication.

[15] using Equation 3 with the stellar rotation $P = 0.72$ days and the known transit duration $D = 29.5$ minutes of TOI-540 b (Ment et al. 2021)

4. DISCUSSION

In the previous section we demonstrated the capability of *nuance* to search for synthetic or known transit signals, in simulated or real datasets. Here, we discuss the caveats of this algorithm, the advantages and limitations of the nuance implementation, and future prospects for its extension.

4.1. *Processing time*

In Figure 16, the processing time of nuance linear and periodic search are recorded against the number of points in a simulated light curve, assuming a simple non-optimized GP with a squared exponential kernel. These are compared to the processing time of `biweight+BLS` (cf. section 3.1) separated into the bi-weight filtering step and the BLS search.

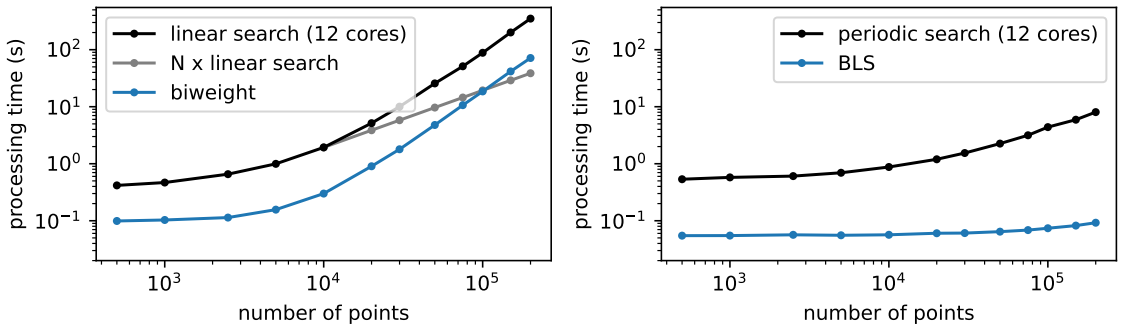

Figure 16. Study of nuance (black line) processing time against `biweight+BLS` (cf. section 3.1, blue line). The gray curve shows the performance of nuance *linear search* when applied to chunks of 10 000 points continuous observations, instead of considering these observations all together. This study is performed on the 12 cores of an Apple M2 Max chip, exploiting the parallelization offered by our implementation. While not being shown, we verify that both the BLS algorithm and *nuance* processing times scale linearly with the number of probed transit durations and orbital periods.

As see in Figure 16, most of the computational costs of nuance and the `biweight+BLS` method in this particular example come from the linear search and the bi-weight filtering step. This is not always true and depends on the size of the trial durations and periods grids. One advantage of *nuance* is that the linear search can be performed separately on different continuous observations, and then combined in the periodic search. Hence, if searching for transits in separate observations with approximately similar durations, such as different TESS sectors or different ground-based nightly observations, the computational cost of nuance grows linearly with the number of observations (see grey line in Figure 16). Nonetheless, considering a variety of other detrending algorithms, **nuance is expected to perform about one order of magnitude slower than more conventional techniques associated with BLS**. The second advantage of nuance is its JAX implementation, allowing the linear search to be run in parallel. As a reference, searching for TOI-540 b transits with nuance

(section 3.3), on the 12 cores of an Apple M2 Max chip, took 5 minutes 35 seconds in total, 1 minute 50 seconds for the 5 sectors linear searches (around 22 seconds each), and 3 minutes 45 seconds for the combined periodic search. In comparison, the brute force search with `biweight+BLS`, consisting in trying 15 bi-weight windows, took a total of 1 minute 49 seconds (about only 7 seconds each).

Because of its computational cost, `nuance` must not be employed in the general case, but rather adopted when light curves contain correlated noise with specific characteristics. If employing a bi-weight filter for detrending, these characteristics correspond to the ones discussed in section 1. But as these strongly depend on the type of detrending technique employed, we do not provide general guidelines as when *nuance* should be preferred over a specific detrending technique. To aid users in making an informed choice of algorithm, extensive benchmarks and guidelines are reserved to future developments and will be progressively shared on `nuance`'s online documentation[16].

4.2. *Systematics modeling*

Throughout the paper, a single column design matrix $\boldsymbol{X}$, corresponding to the mean differential flux (ideally unitary), was employed, hence assuming that the instrumental systematics signals were non-existent. In practice, *nuance* has been developed to linearly model systematic signals through more complex design matrices (as in Foreman-Mackey et al. 2015), in addition with its capability to model correlated noise while searching for transits. This feature is intentionally unexploited in the comparisons presented in section 3, as detrending light curves assuming a linear systematics model, such as PLD co-trending vectors (Deming et al. 2015), is highly incomplete if applied on data while ignoring the presence of other astrophysical signals. Comparisons involving more complex design matrices would also be sensitive to the choice of linear components, and would have unwanted repercussions on their results.

As an illustration, the NEMESIS pipeline (Feliz et al. 2021) starts processing the differential light curves by employing a linear systematics detrending using a least square fit of the data with a reduced PLD basis, before smoothing the signal from stellar variability using an approach similar to the one employed in the `biweight+BLS` approach (cf. section 3.2), hence detrending the systematics with an incomplete model that does not account for stellar variability. To account for stellar variability while fitting the linear systematics model to the data, a step further would be to use a GP, such as done in the EVEREST (Luger et al. 2018) pipeline. However this would also involve some potential degradation of the transit signals (see e.g. Figure 3), with an hardly distinguishable origin. For these reasons, and to keep our comparisons as

[16] https://nuance.readthedocs.io/en/latest/

targeted as possible, we do not compare commonly used systematics detrending approaches and decided to focus our comparisons solely on stellar variability detrending techniques (although these two aspects often overlap in the literature).

Although not being demonstrated here, modeling systematics signals while searching for transits on data acquired sparsly is extremely promising for the search of transiting exoplanets in ground-based data, that usually suffer from daily interruptions. In this respect, we note the similarity of our *linear search* (cf section 2.1) to the one presented in Berta et al. 2012, that focused on the detection of single eclipses in the MEarth light curves (Irwin et al. 2009). Similarly, ***nuance* would highly benefit the search for transiting exoplanets around M-dwarf type stars**, such as the ones observed by the SPECULOOS survey (Gillon 2018) whose monitoring suffers from both increased red noise (due to atmospheric and instrumental thermal effects discussed e.g. in Berta et al. 2012 and Pedersen et al. 2023) and enhanced stellar variability (Murray et al. 2020). We reserve this promising application to a future study.

4.3. *The GP kernel*

While not being discussed in our study, **the efficiency of *nuance* to detect transits in correlated noise is highly dependant on the design of its GP kernel**. In the ensemble comparison of section 3.2, the goal was to choose a kernel and an optimization strategy suited to most of the studied light curves, leading to few outliers in the results that were indicative of a badly designed and/or optimized kernel. An alternative, recommended for more realistic blind searches, is to perform model comparison on well selected kernels, and to adapt the optimization strategy to each dataset.

When using `nuance` on TESS light curves for example, it must be noted that the observed light curve variability might originate from a contaminated photometric aperture, so that a physically-interpretable GP kernel representing a single star activity is not necessarily appropriate. On the other hand, a single squared exponential GP kernel might also be sufficient for some applications.

Something to emphasize is that *nuance* cannot be used to produce reliable detrended light curves, as an optimal GP is often flexible enough to partially model transits (see Figure 3). In contrast, the idea behind *nuance* is rather to compute the likelihood of data against a model containing both transits and correlated noise, without ever trying to disentangle both signals. In practice, it means that it can be very hard to actually verify the presence of transits found by *nuance* visually, so that transits may be detected but remain hidden in correlated noise. This is particularly

true for stars displaying very high-frequency photometric pulsations (see the example in Figure 4.4 where the detrended light curves dismissively follow the base model).

4.4. *Prospects*

The present implementation of *nuance* has the potential to be extended to be used beyond the search of periodic box-shaped transits. Here are ideas of possible use and extensions, from the most straightforward to the most ambitious:

1. In order to compare nuance to BLS-based methods, we injected and retrieved only box-shaped transits. However, similarly to the Transit-Least-Square algorithm from Hippke & Heller (2019), **limb-darkened transits can serve as base model** in the linear search and are expected to improve the transit search in the same way TLS provided an improvement over BLS.

2. The linear search of *nuance* is a single-event detection algorithm that can be used to search for single transit events, but also **detect transiting exocomets and flares**, by simply changing the base astrophysical model in the last colum of the design matrix $\mathbf{X}$. While not being tested and benchmarked, nuance already integrates this feature. An example of the detection of known transiting exocomets in β Pictoris TESS light curves is shown in Figure 4.4.

3. During the periodic search, no prior about the transit duration related to the orbital period of the planet was used. This was done in order to allow the detection of grazing transiting exoplanets that would produce shorter timescale transits compared to what is expected from a circular orbit with a null impact parameter. However, adding such priors might produce less spurious periodogram peaks and be very beneficial for the automatic search of transits in large datasets. Another idea, similar to the one employed in Foreman-Mackey et al. (2015), is to leverage **model comparison in order to reject transits that are better described by the GP model alone**. Both ideas come at no cost given our modeling approach.

4. Finally, the formalism of *nuance* could be adapted and used to **search for exoplanets featuring transit time variations (TTV)**. Indeed, this application only requires a modification of the periodic search, as maximum likelihood peaks close to linearly predicted transit epochs may be considered. This could be done either with a special nearest-neighbor algorithm or with a convolution of the computed likelihood grid with a Gaussian kernel. To maximize efficiency and interpretability, we would recommend these approaches to be explored analytically, rather than using a data-driven treatment of the linear search products.

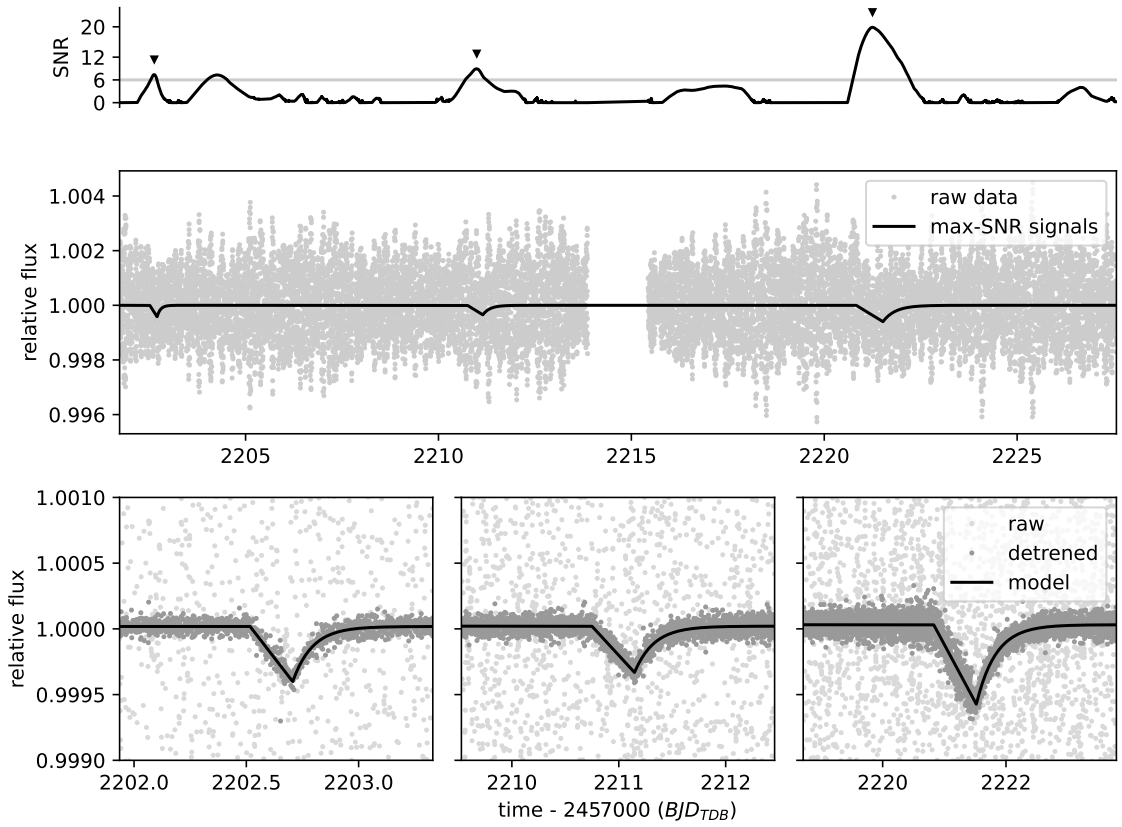

Figure 17. Demonstration of the search of transiting exocomets in the TESS light curves of the star β Pictoris (2 minutes PDCSAP data from sector 33). This star is known to display rapid δ Scuti type photometric variations with a period of about 30 minutes (Lecavelier des Etangs et al. 2022). The GP kernel and its hyperparameters are chosen and optimized as in section 3.2.Here, we simply used the linear search of `nuance` with a different base model, one that mimics the shape of transiting exocomets (with 20 trial durations), to compute the SNR time-series of the signal over one sector. The maximum-SNR events are displayed in the bottom of the figure and match with the ones found by Lecavelier des Etangs et al. (2022).

5. CONCLUSION

This paper presents *nuance*, an algorithm designed to detect planetary transits in light curves featuring correlated noise in the form of instrumental signals and stellar variability. In this context, a conventional approach involves detrending a light curve before searching for transits using a Box-Least-Square algorithm. However, we show that the incomplete modeling of a light curve for its detrending, one that ignores the presence of transits, degrades their signal-to-noise-ratio down to the point of not being detectable. Adopting a widely used detrending strategy, we explore the extent of this degradation on simulated light curves, and its dependance on the photometric stellar variability characteristics, showing the need for a full-fledged transit search method like *nuance*.

The effectiveness of *nuance* is tested using a synthetic dataset and further validated on real TESS light curves of 438 rapidly-rotating M dwarfs. These injection-recovery tests reveal that *nuance* consistently outperforms conventional transit search techniques, especially for transits with a duration exceeding one-fifth of the stellar variability timescale. In all cases, *nuance* not only lead to a higher number of true positive detections but also minimizes false positives, demonstrating its robustness and reliability.

We make *nuance* publicly available through the nuance open-source Python package, developped with JAX to allow its use on distributed computing environments and GPU devices. Overall, we acknowledge the limitations of *nuance* and its increased computational cost compared to more conventional techniques. Hence, *nuance* should be used as an alternative to more traditional techniques only in the presence of substantial correlated noise. As guidelines for choosing our method over other techniques are highly dependant on the type of detrending algorithm employed, we reserve this study to a future work.

Finally, we suggest future improvements and extensions of the algorithm, including its application for detecting single transits, exocomets, flares, and exoplanets featuring transit time variations (TTV), underscoring its versatility and potential for broader impact in astronomical research.

We would like to thank Julien De Wit, Prajwal Niraula for meaningful discussions at the beginning of this project, Germain Garcia for his useful insights about numerical optimization, Michaël Gillon for his overall support, and the member of the Astronomical Data Group at the Center for Computational Astrophysics for many enriching discussions and feedback.

APPENDIX

A. LIGHT CURVES SIMULATIONS

In order to study the effect of correlated noise on transit search, this paper relies on transit light curve simulations including realistic effects of stellar variability and instrumental signals. The following describes how such signals are modeled.

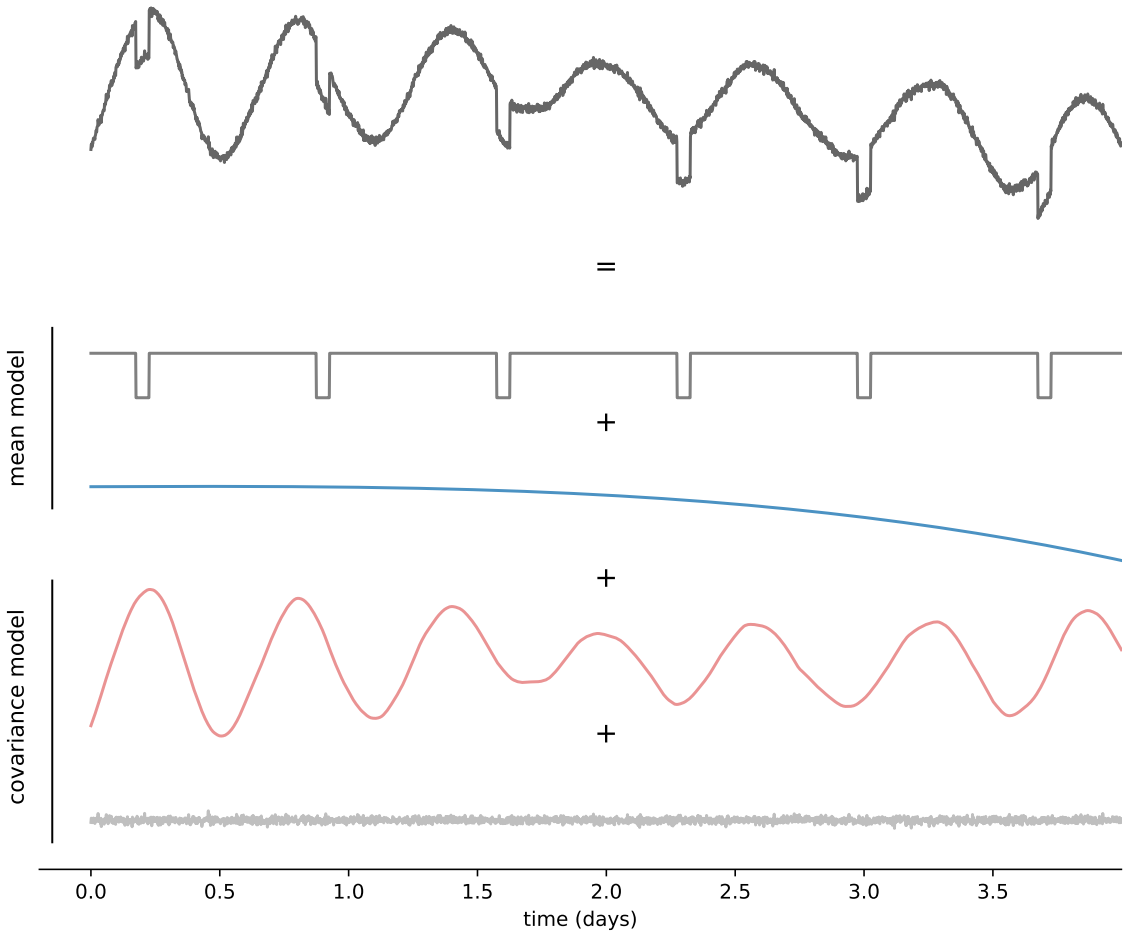

Figure 18. Example dataset sampled at $N = 2880$ times corresponding to an observation of 4 days with an exposure time of 2 minutes. The mean of this signal consists in a periodic transit signal of period $P = 0.7$ days, duration $D = 0.05$ days and depth of 2% ($\mathcal{T}$ in gray) plus instrumental signals ($\mathcal{S}$ in blue). Correlated noise in the form of stellar variability is simulated by modeling the covariance matrix of the signal with a GP ($\mathcal{V}$ in red) including a diagonal variance of 0.001^2 corresponding to white noise (ϵ in light grey). This simulated signal is not intended to be physically realistic.

Let f be the simulated flux of a star sampled and arranged in the vector $\boldsymbol{f}$ associated to the vector of times $\boldsymbol{t}$, such that

$$\boldsymbol{f} \sim \mathcal{N}(\boldsymbol{\mu}, \boldsymbol{C}),$$

i.e. that $\boldsymbol{f}$ is drawn from a GP of mean $\boldsymbol{\mu}$ and covariance matrix $\boldsymbol{C}$. In this equation, $\boldsymbol{\mu}$ is such that its i-th element is defined by $\mu_i = \mathcal{T}(t_i) + \mathcal{S}(t_i)$ where t_i is the i-th time of observation, $\mathcal{T}$ is a periodic transit function and $\mathcal{S}$ a function describing the instrumental part of the signal (both described below). The covariance matrix $\boldsymbol{C}$ is built such that $C_{i,j} = k(t_i, t_j)$ where k is a covariance function (or *kernel*) accounting for correlated noise in the form of stellar variability (with added white noise). An example of such signal is simulated and shown in Figure 18.

A.1. *Transit signal* $\mathcal{T}$

The periodic transit signal $\mathcal{T}$ is simulated using the simple model described in Protopapas et al. (2005), where a transit of period P, epoch T_0, duration D and unitary depth observed at time t is given by

$$\begin{aligned} \mathcal{T}_c(t, P, T_0, D) &= \frac{1}{2}\tanh\left(c\left[\theta - \frac{1}{2}\right]\right) - \frac{1}{2}\tanh\left(c\left[\theta + \frac{1}{2}\right]\right), \\ \text{with} \quad \theta &= \frac{P}{\pi D}\sin\left(\frac{\pi(t - T_0)}{P}\right), \end{aligned} \tag{A1}$$

where the dimensionless parameter c controls the roundness of the transit depth ($c \gg 1$ corresponding to a box-shaped transit as shown in Figure 19). This analytical model is fully empirical but easily differentiable.

Figure 19. Simulations of a single transit signal (Equation A1) shown for different values of c.

In this paper, unless specified, all transits are simulated with $c = 12$, a value arbitrarily chosen that can be fined-tuned in real applications using the limb-darkening coefficients of a given star. The periodic transit signal $\mathcal{T}$ seen in Figure 18 corresponds to $\mathcal{T} = 0.02 \times \mathcal{T}_{c=12}(\boldsymbol{t}, P = 0.7, T_0 = 0.2, D = 0.05)$, all parameters in unit of days.

A.2. *Instrumental signals* $\mathcal{S}$

Instrumental signals are simulated as a linear model of M explanatory variables arranged in the $(N \times M)$ design matrix $\boldsymbol{X}$. Hence,

$$\mathcal{S} = \boldsymbol{X}\boldsymbol{w},$$

where the vector $\boldsymbol{w}$ contains the linear coefficients of the model. The simulated flux shown in Figure 18 contains a linear model where the $M = 4$ columns of the design matrix $\boldsymbol{X}$ are given by $\boldsymbol{X}_i = \boldsymbol{t}^i$ (i.e. $\boldsymbol{X}$ is the Vandermonde matrix order 3 of time t) and $\boldsymbol{w} = [1.0 \quad 0.0005 \quad -0.0002 \quad -0.0005]$.

A.3. *Stellar variability* ν

As this chapter focuses on stellar variability and its effect on transit detection, We employ a simple physically-motivated GP kernel, describing stellar variability through the covariance of a stochastically-driven damped harmonic oscillator (SHO, Foreman-Mackey et al. 2017; Foreman-Mackey 2018) taking the form

$$k(\tau) = \sigma^2 \exp\left(-\frac{\omega\,\tau}{2\,Q}\right) \begin{cases} 1 + \omega\,\tau & \text{for } Q = 1/2 \\ \cosh(f\,\omega\,\tau/2\,Q) + \sinh(f\,\omega\,\tau/2\,Q)/f & \text{for } Q < 1/2 \\ \cos(g\,\omega\,\tau/2\,Q) + \sin(g\,\omega\,\tau/2\,Q)/g & \text{for } Q > 1/2 \end{cases} \tag{A2}$$
$$\text{where} \quad \tau = |t_i - t_j|, \quad f = \sqrt{1 - 4\,Q^2} \quad \text{and} \quad g = \sqrt{4\,Q^2 - 1}$$

where Q is the quality factor of the oscillator, ω its pulsation and σ the amplitude of the kernel function. GP computations in this paper use the implementation from `tinygp`[17], a Python package exposing the quasi-separable kernels from Foreman-Mackey (2018) and powered by `JAX`[18]. The stellar variability signal in Figure 18 has been sampled from a GP with an SHO kernel of parameters $\omega = \pi/6D$ (i.e. a period equal to 12 times the duration D of the simulated transit), $Q = 45$ and $\sigma = 0.02$, the depth of the simulated transit. An extra term $\sigma_f^2 = 0.001^2$ is added to the diagonal of the covariance matrix, corresponding to the variance of the simulated measurement f and leading to the white noise observed in Figure 18.

B. PROOF FOR THE PERIODIC SEARCH EXPRESSION

From the *linear search* presented in section 2.1, we retain and index by k the parameters of the K individual transits whose epochs $\{T_k\}_k$ are compatible with a periodic signal of period P and epoch T_0. From the likelihoods of these transits (computed in section 2.1), we want an expression for

$$p(\boldsymbol{f}|P, T_0, D, \Delta) = \prod_{k \in \mathbb{T}} p(\boldsymbol{f}|T_k, D, \Delta),$$

i.e., given a depth D, the likelihood of the data given a periodic transit signal of period P, epoch T_0 and a common depth Δ. Since only $\{p(\boldsymbol{f}|T_k, D, \Delta_k)\}_k$ is known (i.e. transits with different depths), we decompose

$$p(\boldsymbol{f}|T_k, D, \Delta) = \int p(\boldsymbol{f}|T_k, D, \tilde{\Delta}) p(\tilde{\Delta}|\Delta)\, d\tilde{\Delta}, \tag{B3}$$

where $p(\boldsymbol{f}|T_k, D, \tilde{\Delta})$ is the probability of the k-th transit to have a depth $\tilde{\Delta}$ and $p(\tilde{\Delta}|\Delta)$ the probability to observe the depth $\tilde{\Delta}$ knowing the existence of a common depth Δ. In other words, Equation B3 involves the likelihood of the non-periodic transit k to be part of a periodic transit signal with a common depth Δ.

[17] https://github.com/dfm/tinygp
[18] https://github.com/google/jax

Since each depth Δ_k is found through generalized least square, each follow a normal distribution $\mathcal{N}(\Delta_k, \sigma_k^2)$, centered on Δ_k with variance σ_k^2 and an amplitude $\mathcal{L}_k$, leading to the likelihood function

$$p(\boldsymbol{f}|T_k, D, \tilde{\Delta}) = \mathcal{L}_k \exp\left(-\frac{(\tilde{\Delta} - \Delta_k)^2}{2\sigma_k^2}\right).$$

As for the common transit depth Δ, it can be estimated through the joint probability of all other transit depths than Δ_k, such that

$$\Delta \sim \prod_{i \neq k}^{K} \mathcal{N}(\Delta_i, \sigma_i^2),$$

with

$$\frac{1}{\sigma^2} = \sum_{i \neq k}^{K} \frac{1}{\sigma_i^2} \quad \text{and} \quad \Delta = \sigma^2 \sum_{i \neq k}^{K} \frac{\Delta_i}{\sigma_i^2}. \tag{B4}$$

Hence

$$p(\tilde{\Delta}|\Delta) = \frac{1}{\sqrt{2\pi\sigma^2}} \exp\left(-\frac{(\tilde{\Delta} - \Delta)^2}{2\sigma^2}\right).$$

We can now rewrite Equation B3 as

$$p(\boldsymbol{f}|T_k, D, \Delta) = \frac{\mathcal{L}_k}{\sqrt{2\pi\sigma^2}} \int \exp\left(-\frac{(\tilde{\Delta} - \Delta_k)^2}{2\sigma_k^2}\right) \exp\left(-\frac{(\tilde{\Delta} - \Delta)^2}{2\sigma^2}\right) d\tilde{\Delta}.$$

The integral in this equation is a product of gaussian integrals that can be obtained analytically, leading to

$$p(\boldsymbol{f}|T_k, D, \Delta) = \mathcal{L}_k \sqrt{\frac{\sigma_k^2}{\sigma^2 + \sigma_k^2}} \exp\left(-\frac{1}{2}\frac{(\Delta_k - \Delta)^2}{\sigma_k^2 + \sigma^2}\right).$$

Finally,

$$\ln p(\boldsymbol{f}|P, T_0, D, \Delta) = \sum_{k}^{K} \ln \mathcal{L}_k - \frac{1}{2} \sum_{k}^{K} \left(\ln(\sigma_k^2) - \ln(\sigma^2 + \sigma_k^2) + \frac{(\Delta_k - \Delta)^2}{\sigma_k^2 + \sigma^2}\right), \tag{B5}$$

the log-likelihood of the data given a periodic transit signal of period P, epoch T_0, duration D and common depth Δ. In order to reduce the number of times Equation B4 is computed, we adopt the biased estimates

$$\frac{1}{\sigma^2} = \sum_{k}^{K} \frac{1}{\sigma_i^2} \quad \text{and} \quad \Delta = \sigma^2 \sum_{k}^{K} \frac{\Delta_i}{\sigma_i^2}, \tag{B6}$$

so that Δ and σ are independent of k in the last sum of Equation 8.

C. INJECTION-RECOVERY ON TIC 1019692

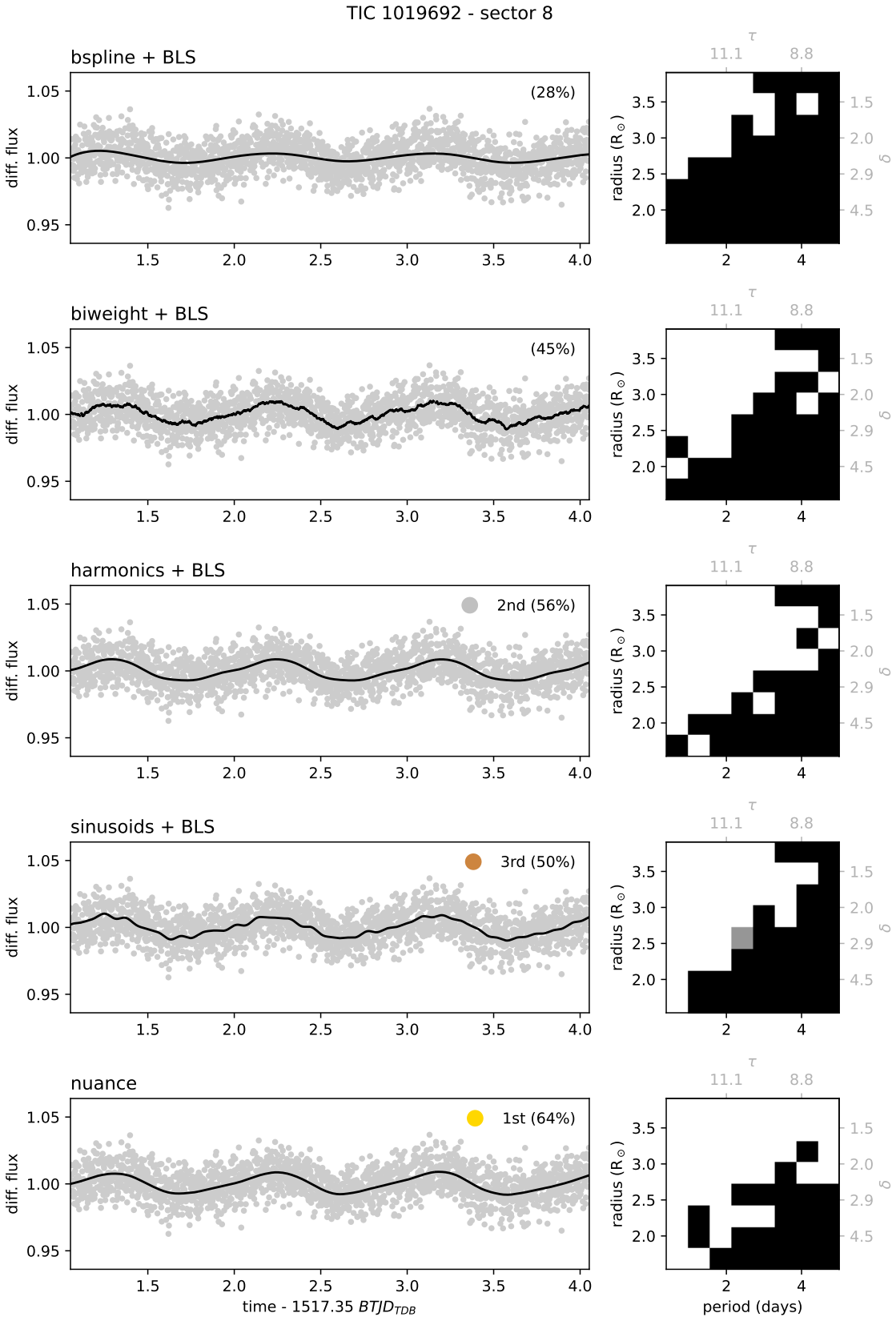

Figure 20. Results of the transits injection-recovery on TIC 1019692 half-sector light curve. Left: cleaned light curve with computed trend overplotted in black (except for nuance where it corresponds to the mean of the GP model). Right: Results of the transit search where a black square denotes a transit signal not detected, gray a signal detected at an alias period ($P/2$ or $2P$), and white a signal detected with the correct period. On the right plots, secondary axes show the (τ, δ) relative parameter space. For each method, the upper right legend on the left plot indicates its ranking based on the percent of recovered transit signals (where a transit with an aliased period counts as being detected).

REFERENCES

Aigrain, S., Parviainen, H., & Pope, B. J. S. 2016, MNRAS, 459, 2408, doi: 10.1093/mnras/stw706

Berta, Z. K., Irwin, J., Charbonneau, D., Burke, C. J., & Falco, E. E. 2012, AJ, 144, 145, doi: 10.1088/0004-6256/144/5/145

Caldwell, D. A., Tenenbaum, P., Twicken, J. D., et al. 2020, Research Notes of the American Astronomical Society, 4, 201, doi: 10.3847/2515-5172/abc9b3

Deming, D., Knutson, H., Kammer, J., et al. 2015, ApJ, 805, 132, doi: 10.1088/0004-637X/805/2/132

Feliz, D. L., Plavchan, P., Bianco, S. N., et al. 2021, AJ, 161, 247, doi: 10.3847/1538-3881/abedb3

Fletcher, R. 1987, Practical methods of optimization: V. 1-2, 2nd edn. (Chichester, England: John Wiley & Sons)

Foreman-Mackey, D. 2018, Research Notes of the American Astronomical Society, 2, 31, doi: 10.3847/2515-5172/aaaf6c

Foreman-Mackey, D., Agol, E., Ambikasaran, S., & Angus, R. 2017, AJ, 154, 220, doi: 10.3847/1538-3881/aa9332

Foreman-Mackey, D., Montet, B. T., Hogg, D. W., et al. 2015, ApJ, 806, 215, doi: 10.1088/0004-637X/806/2/215

Gilliland, R. L., Chaplin, W. J., Dunham, E. W., et al. 2011, ApJS, 197, 6, doi: 10.1088/0067-0049/197/1/6

Gillon, M. 2018, Nature Astronomy, 2, 344, doi: 10.1038/s41550-018-0443-y

Hippke, M., David, T. J., Mulders, G. D., & Heller, R. 2019, AJ, 158, 143, doi: 10.3847/1538-3881/ab3984

Hippke, M., & Heller, R. 2019, A&A, 623, A39, doi: 10.1051/0004-6361/201834672

Howell, S. B., Ciardi, D. R., Giampapa, M. S., et al. 2016, AJ, 151, 43, doi: 10.3847/0004-6256/151/2/43

Irwin, J., Charbonneau, D., Nutzman, P., & Falco, E. 2009, in Transiting Planets, ed. F. Pont, D. Sasselov, & M. J. Holman, Vol. 253, 37–43, doi: 10.1017/S1743921308026215

Jenkins, J. M., Chandrasekaran, H., McCauliff, S. D., et al. 2010, in Society of Photo-Optical Instrumentation Engineers (SPIE) Conference Series, Vol. 7740, Software and Cyberinfrastructure for Astronomy, ed. N. M. Radziwill & A. Bridger, 77400D, doi: 10.1117/12.856764

Kovács, G., Bakos, G., & Noyes, R. W. 2005, MNRAS, 356, 557, doi: 10.1111/j.1365-2966.2004.08479.x

Kovács, G., Hartman, J. D., & Bakos, G. Á. 2016, A&A, 585, A57, doi: 10.1051/0004-6361/201527124

Kovács, G., Zucker, S., & Mazeh, T. 2002, A&A, 391, 369, doi: 10.1051/0004-6361:2002080210.48550/arXiv.astro-ph/0206099

Lecavelier des Etangs, A., Cros, L., Hébrard, G., et al. 2022, Scientific Reports, 12, 5855, doi: 10.1038/s41598-022-09021-2

Lightkurve Collaboration, Cardoso, J. V. d. M., Hedges, C., et al. 2018, Lightkurve: Kepler and TESS time series analysis in Python, Astrophysics Source Code Library. http://ascl.net/1812.013

Luger, R., Agol, E., Kruse, E., et al. 2016, AJ, 152, 100, doi: 10.3847/0004-6256/152/4/100

Luger, R., Kruse, E., Foreman-Mackey, D., Agol, E., & Saunders, N. 2018, AJ, 156, 99, doi: 10.3847/1538-3881/aad230

Ment, K., Irwin, J., Charbonneau, D., et al. 2021, AJ, 161, 23, doi: 10.3847/1538-3881/abbd91

Morris, B. M., Hebb, L., Davenport, J. R. A., Rohn, G., & Hawley, S. L. 2017, ApJ, 846, 99, doi: 10.3847/1538-4357/aa8555

Mosteller, F., & Tukey, J. W. 1977, Data analysis and regression. A second course in statistics

Murray, C. A., Delrez, L., Pedersen, P. P., et al. 2020, MNRAS, 495, 2446, doi: 10.1093/mnras/staa1283

Newton, E. R., Rampalli, R., Kraus, A. L., et al. 2022, AJ, 164, 115, doi: 10.3847/1538-3881/ac8154

Pedersen, P. P., Murray, C. A., Queloz, D., et al. 2023, MNRAS, 518, 2661, doi: 10.1093/mnras/stac3154

Pont, F., Zucker, S., & Queloz, D. 2006, MNRAS, 373, 231, doi: 10.1111/j.1365-2966.2006.11012.x

Pozuelos, F. J., Suárez, J. C., de Elía, G. C., et al. 2020, A&A, 641, A23, doi: 10.1051/0004-6361/202038047

Protopapas, P., Jimenez, R., & Alcock, C. 2005, MNRAS, 362, 460, doi: 10.1111/j.1365-2966.2005.09305.x

Rackham, B. V., Apai, D., & Giampapa, M. S. 2018, ApJ, 853, 122, doi: 10.3847/1538-4357/aaa08c

Ramsay, G., Doyle, J. G., & Doyle, L. 2020, MNRAS, 497, 2320, doi: 10.1093/mnras/staa2021

Rasmussen, C. E., & Williams, C. K. I. 2005, Gaussian processes for machine learning, Adaptive Computation and Machine Learning series (London, England: MIT Press)

Ricker, G. R., Winn, J. N., Vanderspek, R., et al. 2015, Journal of Astronomical Telescopes, Instruments, and Systems, 1, 014003, doi: 10.1117/1.JATIS.1.1.014003

Simpson, E. R., Fetherolf, T., Kane, S. R., et al. 2023, AJ, 166, 72, doi: 10.3847/1538-3881/acda26

Skumanich, A. 1972, ApJ, 171, 565, doi: 10.1086/151310

Tamuz, O., Mazeh, T., & Zucker, S. 2005, MNRAS, 356, 1466, doi: 10.1111/j.1365-2966.2004.08585.x